Paper No. ICONE9051

DEVELOPMENT OF A WEIBULL MODEL OF CLEAVAGE FRACTURE TOUGHNESS FOR SHALLOW FLAWS IN REACTOR PRESSURE VESSEL MATERIAL[1]

B. R. Bass, P. T. Williams, W. J. McAfee, and C. E. Pugh

Heavy-Section Steel Technology Program
Oak Ridge National Laboratory
Oak Ridge, Tennessee 37831, USA

KEYWORDS: Safety - Structural – Vessel

ABSTRACT

A primary objective of the United States Nuclear Regulatory Commission (USNRC) -sponsored Heavy-Section Steel Technology (HSST) Program is to develop and validate technology applicable to quantitative assessments of fracture prevention margins in nuclear reactor pressure vessels (RPVs) containing flaws and subjected to service-induced material toughness degradation. This paper describes a coordinated experimental/analytical program for the development of a Weibull statistical model of cleavage fracture toughness for applications to shallow surface-breaking and embedded flaws in RPV materials subjected to multi-axial loading conditions. The experimental portion includes both material characterization testing and larger fracture toughness experiments conducted using a special-purpose cruciform beam specimen developed by Oak Ridge National Laboratory for applying biaxial loads to shallow cracks. Test materials (pressure vessel steels) included (1) plate product forms (conforming to ASTM A533 Grade B Class 1 specifications) and (2) shell segments procured from a pressurized-water reactor vessel intended for a nuclear power plant that was cancelled. Results from uniaxial and biaxial tests performed on cruciform specimens demonstrated that biaxial loading can have a pronounced effect on shallow-flaw fracture toughness in the lower-transition temperature region. A *local approach* methodology based on a three-parameter Weibull model was developed to correlate these experimentally-observed biaxial effects on fracture toughness. The Weibull model, combined with a new hydrostatic stress criterion in place of the more commonly used maximum principal stress in the kernel of the Weibull stress integral definition, is shown to provide a scaling mechanism between uniaxial and biaxial loading states for 2-dimensional flaws

[1] Research Sponsored by the Office of Nuclear Regulatory Research, U.S. Nuclear Regulatory Commission under Interagency Agreement 1886-N011-9B with the U.S. Department of Energy under Contract DE-AC05-00OR22725 with UT-Battelle LLC. The submitted manuscript has been authored by a contractor of the U.S. Government. Accordingly, the U.S. Government retains a nonexclusive, royalty-free license to publish or reproduce the published form of this contribution, or allow others to do so, for U.S. Government purposes.

located in the A533 B plate material. The Weibull stress density was introduced in the Weibull cleavage fracture model as a metric for identifying regions along a semi-elliptical (3-dimensional) flaw front that have a higher probability of cleavage initiation. Cumulative probability curves generated for RPV shell cruciform specimens indicate a difference in median toughness of 36 MPa$\sqrt{m}$ for the uniaxial (0:1) and biaxial (1:1) loading conditions applied to shallow surface flaws at -60°C.

Introduction

The fracture toughness of shallow surface flaws subjected to biaxial far-field stresses represents an active and important area of research in the field of structural integrity safety assessments of nuclear reactor pressure vessels (RPVs). In the lower-transition temperature region, uniaxial shallow-flaw fracture toughness data [1] for RPV steels exhibit higher mean values and broader scatter bands than are measured for deep flaws under the same loading conditions. This increase in mean fracture toughness has been attributed to a loss of crack-tip constraint due to the close proximity of the crack tip to a free surface of the test specimen [2]. Any increase in crack-tip constraint, for example due to out-of-plane near-surface biaxial stresses, could partially offset this observed trend of shallow-flaw fracture toughness enhancement.

Under pressurized-thermal-shock (PTS) upset conditions, as well as normal pressure-temperature (P-T) operational transients, the thermal, pressure, and residual stresses in an RPV wall are all biaxial (see Figure 1) and combine to form a complex nonlinear biaxial state of stress. Included in this stress field are significant tensile out-of-plane stresses aligned parallel to possible surface or embedded flaws oriented in either the longitudinal or circumferential directions. Standardized fracture toughness testing procedures typically employ specimens such as compact tension, C(T), or single-edge notched bend, SE(B), specimens, that are loaded under a uniaxial state of stress (either tension or bending). Therefore, the resulting fracture toughness data do not reflect the actual biaxial loading state that the postulated RPV flaw will be subjected to in a PTS or P-T transient.

A special cruciform bend specimen (see Figure 2) [3-9] was developed by the Heavy Section Steel Technology (HSST) Program at Oak Ridge National Laboratory (ORNL) to introduce a linear, far-field, out-of-plane biaxial bending stress component in the test section that approximates the nonlinear stresses of PTS or P-T loading. The cruciform specimen permits the application of biaxial loading ratios resulting in controlled variations of crack-tip constraint for shallow surface flaws. The biaxial load ratio is defined as P_T / P_L, where P_T is the load applied to the transverse beam arms and P_L is the load applied to the longitudinal arms. A special test fixture was also designed and fabricated permitting testing under a uniaxial (4-point bending) loading, P_T / P_L ratio of (0:1), and two biaxial (8-point bending) loading ratios, P_T / P_L ratios of (0.6:1) and (1:1). The specimen and test fixture have been described extensively in HSST publications [3-9].

This paper provides a status report on the development and experimental validation of cleavage fracture toughness models for shallow surface flaws located in RPV material and subjected to biaxial loading conditions. An integrated experimental and

analytical approach is used to achieve the program objectives. The experimental portion includes both material characterization testing and larger specialized toughness experiments conducted on the cruciform beam specimen. To make the final products as germane as possible to the evaluation of RPV structural integrity, test materials were selected from the HSST inventory of nuclear pressure vessel steels. These materials included (1) plate product forms (conforming to ASTM A533 Grade B Class 1 specifications) and (2) shell segments from fabricated RPVs. The RPV shell segments were procured from a pressurized-water reactor vessel intended for a nuclear power plant that was cancelled. Thus, the RPV segments are prototypic of materials and fabrication procedures present in operating pressurized water reactors (PWRs). Results from uniaxial and biaxial tests performed on cruciform specimens from these materials demonstrated that biaxial loading can have a pronounced effect on shallow-flaw fracture toughness in the lower-transition temperature region.

A local approach methodology based on a three-parameter Weibull model was developed to correlate these experimentally observed biaxial effects on fracture toughness. The Weibull model, combined with a new hydrostatic stress criterion in place of the more commonly used maximum principal stress in the kernel of the Weibull stress integral definition, has been shown to provide a scaling mechanism between uniaxial and biaxial loading states for 2-dimensional (i.e., straight) surface flaws located in an A533 B plate. The *Weibull stress density* was employed in the Weibull cleavage fracture model as a metric for identifying regions along a semi-elliptical (3-dimensional) flaw front that have a higher probability of cleavage initiation. Fracture probability curves from the latter model predicted a difference in median toughness of 36 MPa$\sqrt{m}$ between uniaxial (0:1) and biaxial (1:1) loading conditions at -60 °C for a shallow 3-dimensional flaw located in a fabrication weld of the RPV shell.

Two-dimensional flaws in heat-treated A533 B material

HSST Plate 14 cruciform testing program

Early experimental studies at ORNL included a series of cruciform bend tests to evaluate biaxial loading effects on the fracture toughness of 2-dimensional shallow surface flaws (straight flaws approximating an infinite-length condition). An A533 B pressure vessel steel, designated HSST Plate 14, was the source material for the initial cruciform bend specimens. The Plate 14 material underwent heat treatment to achieve an elevated yield strength approximating that of a typical radiation-sensitive RPV steel. The heat treatment was performed successfully, providing a room temperature yield stress in the desired range (see Figure 3). From Charpy V-notch testing, T_{CV} was determined to be 56 °C, and the drop-weight nil-ductility temperature (*NDT*) was found to be 40 °C. Thus, *NDT* controlled the reference temperature, and RT_{NDT} = 40 °C. A series of compact tension, C(T)-1/2T, specimens, taken from different locations within the parent plate, were used to determine a reference temperature T_0 = -50.9 °C based on the *Master Curve* approach [10].

The initial cruciform bend specimens were fabricated with the test section having dimensions of 104 mm × 104 mm × 104 mm and a 2-dimensional shallow flaw with a flaw-to-depth ratio of $a/W = 0.1$ (see Figure 2). The flaw was located in material near the mid-plane of the original plate. Load-diffusion control slots (LDCS) were machined into the specimen loading arms to create boundary conditions required to achieve a uniform stress field in the central test section. For each cruciform specimen, the shallow 2-dimensional flaw was fatigue-sharpened and a mechanical milling process was used to relieve each corner of the sharpened flaw and remove a small region of material at the LDCS/flaw intersection. That region had exhibited preferential crack growth during the fatiguing process due to prior surface embrittlement resulting from wire electron-discharge-machine (EDM) fabrication of the LDCS. Next, the transverse loading arms were attached by electron-beam (EB) welding. The specimen design, coupled with a statically-determinate load-reaction system installed in the ORNL testing machine, permitted the specimen to be loaded in either uniaxial (4-point bending) or biaxial (8-point bending) configurations. Tests of nominally identical specimens could therefore be performed with the level of stress biaxiality as the only loading test variable.

A basic functional requirement for the cruciform bend test specimen was that stresses in the ligament beneath the shallow flaw remain in the elastic range up to the point of fracture, thus maintaining a condition of "well-contained" yielding within the vicinity of the flaw front. The technical basis for this requirement arises from the following observations: (1) well-contained yielding is the condition present in the RPV wall during a PTS transient and (2) previous biaxial experimental studies [11] have shown that when substantial plastic strains are allowed to develop in the ligament, the effects of biaxial loading on fracture toughness are lost. Extensive experimental and analytical studies [12] confirmed that the ORNL cruciform specimen satisfied these requirements.

Instrumentation applied to the test specimens included thermocouples, strain gages, clip gages, and displacement transducers. Both crack-mouth-opening displacement (CMOD) and load-line displacement (LLD) were monitored continuously throughout each of the tests. Control of the test temperature was achieved with various liquid nitrogen distribution systems. Mechanical loading was applied to the cruciform specimens using a large-scale cruciform test fixture mounted in a 3.1 MN Instron servo-hydraulic testing machine located at ORNL.

Six cruciform specimens were tested at -30 °C to provide data for (a) three biaxial load ratios and (b) two duplicate tests at each condition. At this temperature, the specimens exhibited very little plastic deformation as measured by both CMOD and LLD, regardless of the applied biaxial load. For cases where primarily elastic deformation occurs, biaxial loading would be expected to have little effect on constraint at the flaw tip, and thus little effect on toughness. The elastic response of these specimens gave an indication that the test temperature was too low to produce a biaxial loading effect (i.e., -30 °C was on or nearly on the lower shelf).

A second set of fifteen cruciform specimens was tested at a nominal test temperature of -5 °C. This higher temperature was expected to provide a better balance between cleavage behavior and accumulated plasticity at failure for

evaluation of biaxial effects on toughness. Six specimens each were tested under uniaxial (0:1) and equibiaxial (1:1) loadings, and three specimens under (0.6:1) biaxial loading. Deformation responses of longitudinal load versus CMOD results are shown in Figure 4. The longitudinal load versus CMOD traces for these specimens were comparable, but the failure deformation magnitudes and scatter exhibited a strong dependence on the applied biaxial load as shown in Figure 4.

Three-dimensional elastic-plastic finite element analyses of the cruciform specimen were performed with the ABAQUS program [13] to generate η-factors for determination of fracture-toughness values from test data [12]. The estimated toughness values obtained from the Plate 14 cruciform specimens are shown graphically in Figures 5 and 6 for the -30 °C and -5 °C test sets, respectively. The -30 °C specimens behaved in an elastic manner and little biaxial effect was observed. For the six specimens tested, the toughness increased slightly with an increase in biaxial ratio. It is expected that additional specimens would show statistically no difference between uniaxial and biaxial loading at this temperature. For the tests performed at -5 °C, the test data demonstrate a significant effect of biaxial loading on shallow-flaw fracture toughness, as is shown in Figure 6. The mean value of the biaxial (1:1) toughness resulted in approximately a 35 percent decrease from the mean uniaxial toughness ($\bar{K}_{Jc(1:1)}/\bar{K}_{Jc(0:1)} = 0.65$). In terms of the median of the data sets, the decrease was 41 percent ($K_{med-Jc(1:1)}/K_{med-Jc(0:1)} = 0.59$). The statistical significance of the observed difference in sample means ($\bar{K}_{Jc(0:1)} - \bar{K}_{Jc(0:1)} = 106.3\text{MPa}\sqrt{\text{m}}$) can be estimated with a two-sample comparison of the means. The critical and fundamental assumption of statistical independence of the sample data is made. The application of the *t* statistic also requires the assumption of normal parent populations; however, the procedure is robust in the presence of non-normalcy due to the *Central Limit Theorem* and the use of linear statistics. A one-sided test based on the difference of the means asserts a *null hypothesis* which states that the two samples represent random drawings from the same parent population, $H0: \mu_{(0:1)} - \mu_{(1:1)} = 0$, against the alternative hypothesis, $H1: \mu_{(0:1)} - \mu_{(1:1)} > 0$. For 10 degrees of freedom ($\nu = n_{(0:1)} + n_{(1:1)} - 2$), the resulting heteroscedastic *t*-statistic ($t_{10} = 2.656$) produces a *p*-value of 0.0121, i.e., the probability that the *null hypothesis* is true is only 1.21%, and the *null hypothesis* is rejected. The test data therefore support the contention that the biaxial effect indicated by the trends of the means of the uniaxial (0:1) and biaxial (1:1) toughness data in Figure 6 is statistically significant.

Weibull Model of Cleavage Fracture Toughness

The effects of biaxial loading on cruciform shallow-flaw fracture toughness data in the lower-transition temperature region were studied using the Weibull methodology implemented in the WSTRESS (Version 2.0) computer code [14]. The WSTRESS code employs a multi-axial form of the *weakest-link* model applicable for a 3-dimensional cracked solid; the Weibull stress, σ_w, is characterized as a fracture parameter reflecting the local damage of the material near the crack tip. The Weibull stress, σ_w, given by the expression

$$\sigma_w = \left[\frac{1}{4\pi V_0} \int_{\Omega} \int_{0}^{2\pi} \int_{0}^{\pi} \sigma_q^m \sin\varphi \, d\varphi \, d\theta \, d\Omega \right]^{\frac{1}{m}} \quad (1)$$

is evaluated by integration of the equivalent stress, σ_q, over the process zone. In Eq. (1), V_0 is a reference volume; m is the Weibull modulus; θ and φ are curvilinear coordinates for integration of the tensile stress; and Ω denotes the volume of the near-tip fracture process zone, defined as the volume within the contour surface $\sigma_1 \geq \lambda\sigma_0$, where σ_1 is the maximum principal stress and σ_0 is the yield stress. The cut parameter λ is nominally set to 2 to ensure that all material points within the active process zone have undergone plastic deformation, as recommended in [14].

A fracture criterion must be specified to determine the equivalent (tensile) stress, σ_q in Eq. (1), acting on a microcrack included into the fracture process zone. Three options for fracture criteria are implemented in the distributed version of WSTRESS [14] to evaluate the critical stress at which the crack becomes unstable: (1) maximum principal stress (MPS), (2) coplanar energy release (CER) rate, and (3) normal stress averaging (NSA). Three additional fracture criteria were added to WSTRESS: (4) the principal of independent action (PIA) [15] as proposed by Dortmans et al. [16], (5) the noncoplanar energy release (NCER) rate [17-18], and (6) the hydrostatic stress (HYDRO) criterion developed during the present study. As reported in [19], the first five criteria shared an insensitivity to the effects of biaxial loading due to the dominant role of the opening-mode stress in their definitions. Of the six criteria studied, only the hydrostatic stress criterion, where $\sigma_q = I_1/3 = \sigma_H$ (I_1 is the first invariant of the Cauchy stress tensor), showed a consistent response to biaxial loading. In this paper, the MPS criterion, where $\sigma_q = \sigma_1$, is applied as representative of the group of (1)-(5) criteria in comparisons with the HYDRO criterion. See [9,19] for detailed comparisons of these criteria.

After applying a calibration procedure [20] to determine the required model parameters (the Weibull shape parameter, m, and scale parameter,σ_u) for the HSST Plate 14 material and test temperature, the sensitivity of the Weibull stress (for the cruciform specimen) to variations in loading and constraint levels is shown in Figure 7 for two definitions of the equivalent stress, σ_q, in Eq. (1). In Figure 7(a), the conventional definition using the maximum principal stress demonstrates a sensitivity to constraint variation due to relative flaw depth but not due to biaxiality. The C(T) load path in Figures 7(a) and (b) is based on a deep flaw ($a/W = 0.5$), and the cruciform load paths (x:1) are based on a shallow flaw ($a/W = 0.1$), all with a 1T flaw length. The Weibull stresses in Figure 7(b) are calculated using the hydrostatic stress as the equivalent stress, and the sensitivity to constraint variations due both to relative flaw depth and to biaxial loading state is evident.

The cumulative probability of failure by transgranular cleavage P_f can be estimated by a three-parameter Weibull distribution [21] of the form

$$P_f(\sigma_w) = 1 - \exp\left[-\left(\frac{\sigma_w - \sigma_{w\text{-min}}}{\sigma_u - \sigma_{w\text{-min}}} \right)^m \right] \quad (2)$$

where the parameters of the distribution are the Weibull modulus m (shape parameter), the scaling stress (scale parameter) σ_u , and the minimum Weibull stress for cleavage fracture $\sigma_{w\text{-}min}$ (location parameter). The probability of failure may also be expressed as a function of the fracture parameter, J_c, with a three-parameter Weibull distribution

$$P_f(J_c) = 1 - \exp\left[-\left(\frac{J_c - \gamma}{\beta - \gamma}\right)^{\alpha}\right] \tag{3}$$

where α, β, and γ are the shape, scale, and location parameters of the distribution, respectively. The shape and scale parameters (α,β) were estimated by the *maximum-likelihood* method using the cruciform toughness data. The threshold parameter γ is assumed to be 2.05 kJ/m^2 corresponding to a K_{min} of 20 MPa$\sqrt{m}$ employed in the *Master Curve* model [10]. The associated Weibull probability density function is given by

$$f(J_c,\alpha,\beta,\gamma) = \frac{\alpha}{\beta - \gamma}\left(\frac{J_c - \gamma}{\beta - \gamma}\right)^{\alpha-1} \exp\left(-\left(\frac{J_c - \gamma}{\beta - \gamma}\right)^{\alpha}\right) \tag{4}$$

A calibration scheme was proposed by Gao, Ruggieri, and Dodds [20] (designated herein as the G-R-D Method) to determine unique values of the Weibull parameters (m,σ_u) by applying toughness data measured under low and high constraint conditions at the crack front. They demonstrated analytically and numerically that calibration schemes based only on toughness data from high-constraint specimens under small-scale-yielding (SSY) conditions produce non-unique values of the Weibull parameters. The new G-R-D calibration scheme eliminates this non-uniqueness by mapping the available toughness data at two levels of constraint back to an SSY Weibull stress space where α [in Eq. (3)] takes on the theoretical values of 2 or 4 for Weibull distributions expressed in terms of J_c or K_{Jc}, respectively. In SSY space, the scale parameter (β) can be uniquely determined by iteration on the Weibull shape parameter, m.

In addition to elastic-plastic analyses of large-scale yielding (LSY) specimens, the G-R-D calibration scheme also requires the results of a finite-element analysis of a stationary crack under SSY conditions. The plane-strain, modified boundary layer (MBL) model [22,23] provides asymptotic crack-tip stress fields. For applications described herein, an MBL finite-element model was employed utilizing Plate 14 material property data for -5 °C to calculate SSY solutions corresponding to an applied Mode I loading of the finite-root-tip crack. Details of the G-R-D calibration scheme are given in [20], and its application to cruciform toughness data is described in [9,19]. In summary, the G-R-D scheme proceeds by the following steps:

Step 1. Test two sets of specimens (both under LSY conditions) with different levels of crack-tip constraint. In the terminology of [20], the biaxial (1:1) data are designated as Configuration A (high constraint), and the uniaxial (0:1) data are designated as Configuration B (low constraint).

Step 2. Perform detailed 3-dimensional finite-element analyses for Configurations A and B and for a plane-strain SSY model with a reference thickness adjusted to be consistent with the specimens in Configurations A or B.

Step 3. Assume a trial m-value, and calculate the σ_w versus J histories for Configurations A and B and the SSY model. Constraint-correct the Configuration A and B toughness data by mapping the data points on the σ_w versus J curves back to the SSY curve as shown in Figure 8a such that $J_{c\text{-}(i)} \rightarrow J_{(i)\text{-}SSY}$ for $\sigma_{w(x:1)} = \sigma_{w\text{-}SSY}$.

Step 4. Estimate $\beta_{(0:1)}$ and $\beta_{(1:1)}$ in SSY Weibull stress space for the two configurations by the maximum-likelihood point estimate relation (without small-sample bias) for a sample size n

$$\beta = \sqrt{\frac{1}{n}\sum_{i=1}^{n}\left(J_{(i)\text{-}SSY}\right)^2} \tag{5}$$

and calculate a relative error with the error function $R(m)$,

$$R(m) = \frac{\left(\beta_{(0:1)} - \beta_{(1:1)}\right)}{\beta_{(0:1)}} \tag{6}$$

Step 5. Repeat Steps 3 and 4 for a range of trial m-values and determine the m-value that produces an acceptably small relative error $R(m)$ (see Figures 8b and 8c). The scaling stress, σ_u, can then be calculated from the converged ($\sigma_{w\text{-}SSY}$ versus J) curve by

$$\sigma_u = \sigma_{w\text{-}ssy} @ J_{SSY} = \beta_{(0:1)} = \beta_{(1:1)} \tag{7}$$

For the 3-parameter Weibull distribution, the location parameter, $\sigma_{w\text{-}min}$, is calculated from the intercept of the SSY-($\sigma_{w\text{-}SSY}$ versus J) curve at $J = 2.05$ kJ/m^2 ($K_J = 20$ MPa$\sqrt{m}$ using a plane-strain conversion relation).

The G-R-D scheme represented by Steps 1-5 above was employed to determine parameters for the Weibull model based on the HYDRO criterion for cleavage fracture. With the C(T) specimen (12 data points) as Configuration A and the uniaxial (0:1) specimen (6 data points) as Configuration B, the resulting Weibull parameters were (m, σ_u) = (10.2, 2154 MPa). For the three-parameter Weibull model, the third parameter $\sigma_{w\text{-}min}$ was determined to be 1040 MPa from the $\sigma_{w,SSY}$ versus J curve at $J_{min} = 2.05$ kJ/m^2 ($K_{min} = 20$ MPa$\sqrt{m}$).

Figure 9 presents plots of the resulting failure probabilities calculated by Eq. (2) for the two data sets used to calibrate the model (Figure 9a for C(T) and Figure 9c for uniaxial (0:1)). Failure probabilities for the equibiaxial (1:1) condition, representing an intermediate constraint level not employed in the calibration, are shown in Figure 9b. The median rank probabilities assigned to the toughness data were calculated using the following estimate [24] for the ith data point in a sample of n data points

$$P_{i-rank} = \frac{i-0.3}{n+0.4} \tag{8}$$

where the toughness data are ranked according to increasing magnitude. The 90 percent confidence limits on the median rank probability estimates were determined with an algorithm presented in [25].

With the Weibull statistical fracture model calibrated, a toughness biaxial scaling model was then constructed and expressed in several graphical forms as shown in Figures 10 and 11. In Figure 10a, the ordinate is the *J*-integral normalized by the value of β_{SSY} obtained from the converged solution in the G-R-D calibration scheme. Curves of $J_{(x:1)}/\beta_{SSY}$ for the different biaxial ratios (i.e., constraint levels) are plotted as a function of the normalized Weibull stress serving as the fracture parameter. For a given probability of failure, P_f , Eq. (2) can be inverted to calculate the corresponding critical Weibull stress

$$\frac{\sigma_w{}^*}{\sigma_u{}^*} = \frac{\sigma_w - \sigma_{w-\min}}{\sigma_u - \sigma_{w-\min}} = \left[-\ln(1-P_f)\right]^{\frac{1}{m}} \tag{9}$$

As shown in Figure 10a for a $P_f = 0.5$, the intersection of the vertical line of constant Weibull stress with the $J_{(x:1)}/\beta_{SSY}$ curves gives the scaling of the various constraint levels for the same probability of failure. Traversing a range of failure probabilities allows the construction of Figure 10b where the abscissa is the normalized uniaxial $J_{(0:1)}/\beta_{SSY}$.

The scaling model may also be expressed in terms of toughness ratios as in Figures 11a and 11b. Ratios of stress intensity factors can be calculated from *J*-integral ratios by

$$\frac{K_{Jc(x:1)}}{K_{Jc(0:1)}} = \sqrt{\frac{J_{c(x:1)}}{J_{c(0:1)}}} \tag{10}$$

In Figure 11a, the ratio $K_{Jc(x:1)}/K_{Jc(0:1)}$ is plotted as a function of $K_{Jc(0:1)}$. The C(T) curve can be seen to follow very closely the biaxial (2:1) cruciform curve in Figure 11a. The ratio of the median toughness $K_{Jc\text{-}med(x:1)}/K_{Jc\text{-}med(0:1)}$ at the failure probability $P_f = 0.5$ can be plotted as a function of the biaxial ratio. In Figure 11b, the predicted biaxial scaling model curve for the median failure probability of $P_f = 0.5$ is compared to the medians of the cruciform normalized by the median toughness of the uniaxial (0:1) specimen predicted by the scaling model. Good agreement at $P_T/P_L = 0$ is not unexpected since the uniaxial (0:1) data were used in the calibration of the model. The fact that the data at $P_T/P_L = 0.6$ and $P_T/P_L = 1.0$ also show good agreement with the biaxial scaling model, however, provides encouraging evidence of the validity of the analysis, since these data were not used in the model calibration.

SHALLOW SURFACE FLAWS IN RPV SHELL MATERIAL

RPV Shell Cruciform Testing Program

The RPV shell cruciform test program was initiated as a follow-on task to the Plate 14 cruciform test series [8-9,19]. The plate material is A533 B steel with a stainless-

steel strip-clad overlay on the inner surface. Two shell segments, measuring approximately 3890 mm in the axial direction, and 1370 mm in the circumferential direction, were acquired. Each shell segment included two circumferential welds and one longitudinal weld. The longitudinal weld was of the double-J geometry and ran from the "upper" circumferential weld through the lower end of the shell segment. The vessel was cut such that the longitudinal weld was located near the mid-width of the shell segment. The welds were submerged-arc welds (SAWs) with A 533 B Class 1 filler metal. The plate material, clad overlay, and weldment are typical of a production-quality RPV. The shell had a nominal inner radius of 2210 mm (87 in.) and a thickness of 232 mm (9.125 in), which includes ~5 mm of clad overlay. The cruciform specimens tested in this series were constructed with surface flaws extending into the fabrication weld material from this RPV shell.

Characterization studies of the component materials in the RPV shell, i.e., the fabrication welds, clad layer, clad/HAZ region, and plate material, included tensile tests, Charpy V-notch (CVN) tests, drop-weight tear (DWT) tests, RT_{NDT} and T_o determinations, and fracture toughness determinations from CT and SE(B) specimens; detailed results are reported in [12]. These tests showed little difference in the mechanical properties of the circumferential and longitudinal welds. The longitudinal weld appears to be slightly tougher than the circumferential weld, but both welds have similar strengths, impact properties, nil-ductility (NDT) temperatures, and fracture toughness. Figure 12 depicts the stress-strain response from the component materials measured at –30 °C using round-bar and sheet-type tensile specimens.

Companion shallow- and deep-flaw SE(B) specimens were tested to provide the fracture toughness data under low- and high-constraint conditions needed for a Weibull model calibration using the G-R-D scheme. Eight shallow-flaw specimens and eight deep-flaw specimens were removed from the RPV longitudinal weld. The specimen design was a standard ASTM 1T SE(B) specimen with the exception that the final a/W ratio for the shallow-flaw specimens was 0.2 . A test temperature of T = -62 °C was selected for both specimen types; for the longitudinal weld material, RT_{NDT} = -60 °C. The toughness values were calculated using the ASTM E1921 procedure [10]. The η-factors required for fracture toughness determinations from the SE(B) specimens were computed from three-dimensional finite-element analyses of each geometry. The resulting toughness values for the deep-flaw specimens are shown in Table 1 and those for the shallow-flaw specimens in Table 2.

Intermediate-scale cruciform specimens, measuring 104-mm (4-in.) in thickness, were cut from the inner (clad) surface of the RPV shell containing the longitudinal weld, shown schematically in Figure 13. Two phases of the fabrication sequence for these specimens are shown pictorially in Figure 14. A finite-length semi-elliptical (or 3-dimensional) surface flaw was inserted into the test section of the longitudinal beam configuration (shown in Figure 14a), through the inner (clad) surface, using a shaped electrode and the EDM process. Then, the flaw was extended approximately 1.2 mm around its entire periphery by fatigue loading. After fatigue pre-cracking, the flaw had a depth, a, and surface length, 2ℓ, dimensions of 19 mm and 53 mm, respectively. The test flaw was oriented with its major axis parallel to the direction of the fabrication weld deposition. The leading edge of the flaw passed through the clad

layer, the clad/HAZ, and into the fabrication weld. Finally, transverse beam arms were EB welded onto the longitudinal beam to achieve the cruciform configuration shown in Figure 14b.

Tests of RPV cruciforms were performed to provide a data base for validation of a Weibull model of cleavage fracture for 3-dimensional surface flaws. Ideally, a minimum of six specimens would be tested under uniaxial loading and six under biaxial loading, at a single temperature in the lower-transition region of the weld material. That number of tests could provide a credible data set for application of order statistics in the assessment of probabilistic models of fracture (described in the previous section). However, only six longitudinal weld cruciform specimens were provided for the validation study at a single test temperature, four of which were tested under (1:1) biaxial loading and two under (0:1) uniaxial loading. All six specimens were tested at temperatures near –62 °C, resulting in normalized temperatures of $T - RT_{NDT}$ = (-62 - (-60)) = -2 °C, and $T - T_o$ = (-62 - (-68)) = +6 °C.

The test procedures and instrumentation for these specimens were the same as those used for the Plate 14 cruciform tests described in the previous section. The test results are summarized in Table 3. Fractographic examinations were performed on the fracture surfaces to verify the amount of flaw growth during fatigue pre-cracking, to determine the amount of ductile tearing (if present), and to measure the location of the cleavage initiation site(s). Typical fracture surfaces are shown in Figure 15a and 15b for specimens tested under uniaxial (0:1) and biaxial (1:1) loading, respectively. Location of the cleavage initiation site(s) was observed to be dependent upon the biaxial loading ratio. Uniaxially (0:1) loaded specimens tended to initiate near the deepest point along the flaw tip, while biaxially (1:1) loaded specimens tended to initiate near the interface between the clad/HAZ and fabrication welds.

Weibull Model of Cleavage Fracture for Shallow Surface Flaws

The SE(B) specimens from RPV longitudinal weld material provided data for calibration of a Weibull cleavage fracture model based on hydrostatic stress. Eight shallow-flaw (a/W = 0.2) and eight deep-flaw (a/W = 0.5) SE(B) 1T specimens were tested at a single test temperature to provide comparative toughness data between shallow- and deep-flaw behavior. The calibration procedure required the development of four finite-element models, sharp-tip and blunt-tip models for each of the two specimen geometries. Essential elements and results of the calibration procedure are summarized in Figure 16.

The concept of *Weibull stress density* was introduced into the Weibull cleavage fracture model as a metric for identifying regions along the 3-dimensional flaw front that have a higher probability of cleavage initiation. The Weibull stress density calculations were performed using the ORNL-developed ORWED (Oak Ridge WEibull Stress Density) computer program. ORWED is based on a formulation developed by Gao and Dodds [21]. They introduced a Weibull stress density function ($\bar{\sigma}_w$) defined by

$$\bar{\sigma}_w^m(z) = \frac{1}{V_0} \int_{\bar{A}(z)} \sigma_1^m dz \tag{11}$$

where σ_1 is the maximum principal stress, m is the calibrated shape parameter of the Weibull model, and $\bar{A}(z)$ is the area of the local fracture process zone at the plane z = constant, such that the complete process zone volume is given by

$$\bar{V} = \int_{-B/2}^{+B/2} \bar{A}(z) dz \,, \tag{12}$$

where B is the thickness of a bend-bar specimen with a straight crack front. The global Weibull stress is then defined by

$$\sigma_w = \left[\int_{-B/2}^{B/2} \bar{\sigma}_w^m(z) dz \right]^{\frac{1}{m}} , \tag{13}$$

where the Weibull stress-density function $\bar{\sigma}_w$ depends implicitly on the local J-integral at crack-front position z through the maximum principal stress, σ_1.

In the ORWED program, the Weibull stress density was generalized for curved crack fronts with multiaxial loading. Figure 17 shows a schematic of a semielliptical surface crack of depth a and width $2l$ with a layer of cladding along the inner surface. The crack front can be expressed mathematically as a semi-elliptic arc of length $2s$. Taking advantage of symmetry, one half of the crack front is approximated by the sum of a series of discrete line segments Δs_i. At each discrete position, a plane, A_i, is defined whose normal is equal to the tangent vector at position $\vec{s}_i$ (see Figure 17). The sub-volume ΔV_i is that volume bounded by A_i and A_{i+1} and the outer bounding planes of the model. A local fracture-process zone $\Delta\Omega_i$ can now be defined as the volume contained within ΔV_i such that

$$\Delta\Omega_i = \{\Delta V_i \,|\, \sigma_\Omega \geq \lambda\sigma_0\} \tag{14}$$

where conventionally $\sigma_\Omega = \sigma_1$, $\lambda \approx 2$, and σ_0 is the yield stress. With this definition of a local fracture-process zone, the generalized Weibull stress density at the discrete position $\vec{s}_i$ on the crack front is now given by

$$\bar{\sigma}_w^m(s_i) = \frac{1}{V_0} \int_{\Delta\Omega_i} \frac{\sigma_q^m}{|\Delta s_i|} d\Omega \,, \tag{15}$$

where, for the case of multiaxial loading, the equivalent tensile stress is the hydrostatic stress, $\sigma_q = \sigma_H$. Given the calculated profile of the Weibull stress density along the crack front, the global Weibull stress can be determined from

$$\sigma_w = \left[2\int_0^s \bar{\sigma}_w^m(s)ds \right]^{\frac{1}{m}} \approx \left[2\sum_{i=1}^{n} \bar{\sigma}_w^m(s_i)\Delta s_i \right]^{\frac{1}{m}} . \quad (16)$$

Figure 18 depicts a blunt-tip finite-element 1/4 model of the cruciform with bending loads applied as uniform surface pressures at ends of longitudinal and transverse beam arms. A rigid contact surface under the test section completes the statically-determinate boundary conditions that simulate 8-point bending. In Figure 19, elements of that cruciform model have been partitioned into discrete regions along the flaw front to carry out the Weibull stress density calculations. Figure 20 shows the variation of normalized Weibull stress density plotted as a function of distance measured from the symmetry plane below the clad layer for a beam subjected to uniaxial moment loading of 143.1 kN-m; peak values occur near the maximum flaw depth. In Figure 21, biaxial (1:1) loading is seen to produce a relative uniform distribution of the normalized Weibull stress density along the flaw front for lower applied loads. At the highest load, peak values of the Weibull stress density occur in the near-surface region of base metal, i.e, near the clad heat-affected zone. Thus, a transition from uniaxial to biaxial loading leads to a substantial shift in location of the calculated maximum Weibull stress density for the clad cruciform. Inspection of fracture surfaces from clad cruciform tests (see for example Figures 15a and 15b) have produced experimental data that are consistent with the shift in location of cleavage initiation sites (due to a transition from uniaxial to biaxial loading) predicted by the Weibull stress density model.

An applied K_J (or J) is computed as an averaged value over a portion of the flaw perimeter where the Weibull stress density assumes near-peak values. That averaged parameter is used in conjunction with the Weibull cleavage fracture model to predict probability of initiation for shallow surface flaws in the clad cruciform beams. In Fig 22, applied longitudinal load versus applied $\overline{K_J}$ is plotted for clad cruciform beam specimens tested under uniaxial (0:1) and biaxial (1:1) loading at – 60 °C. The applied $\overline{K_J}$ represents an averaged value taken over a region of the flaw perimeter where the Weibull stress density assumes near-peak values for each of the two loading cases. Figures 20 and 21 indicate where on the flaw perimeter (corresponding approximately to the region where the Weibull density was greater than 90 percent of the peak value) the averaging was carried out.

It should be noted that, while the designated region for determining $\overline{K_J}$ in the uniaxial loading case generally corresponded to the region near the peak applied K_J at the deepest point of the flaw, in the biaxial (1:1) loading case the two regions of peak Weibull density and peak applied local K_J did not necessarily coincide. Over much of the range of biaxial (1:1) loading levels, the applied local K_J was approximately uniform over the base weld material with the peak K_J located near the HAZ/clad interface. The Weibull density was also nearly uniform in this base weld region at lower load levels, establishing a definitive peak only with higher loading as shown in Figure 21. This Weibull density peak was located in a region below the HAZ/base interface and below the location of the peak K_J.

Linkage between the applied loading (expressed in terms of J or K) and the cumulative probability of initiation for a given biaxial constraint condition is depicted in the schematic diagram of Figure 23. The three major elements of that diagram are described as follows:

(A) Finite-element modeling analyses of the flawed structure establish the unique functional relationship between the applied load (J or K_J) and the Weibull stress, σ_w, for a given constraint condition. The Weibull stress distribution along the flaw front is computed using the ORWED program and the Weibull model parameters determined from the calibration procedure based on shallow- and deep-flaw bend bar data. The applied load J (or K_J) values are determined from the averaging process taken over a region of peak Weibull stress density (described above).

(B) The cumulative probability of initiation, P_f, as a function of σ_w is completely defined by the Weibull model parameters calibrated for a specific material and temperature from the bend-bar data.

(C) The relations established in steps (A) and (B) provide the unique linkage between P_f and applied J or K_J for the given variables of structural flaw geometry, loading, material properties and temperature.

Application of these procedures to analysis of the RPV clad cruciform beam specimen is illustrated in Figures 24-26. Sharp-tip and blunt-tip finite element models of the cruciform specimen containing a finite-length surface flaw in the RPV fabrication weld material (and cladding) were constructed and analyzed for uniaxial and biaxial loading conditions. These analyses provided input to the ORWED program for the generation of normalized Weibull stress versus normalized applied J curves for uniaxial (0:1) and biaxial (1:1) loading conditions. The Weibull model parameters used in these analyses are those determined from the calibration procedure based on shallow- and deep-flaw bend bars. The small-scale yielding solution for the weld material is shown in the plot for reference. Fracture toughness data obtained from a series of six clad cruciform tests conducted near –60 °C under uniaxial and biaxial loading are also included in the plot; additional details concerning those data are given in Table 3. Cumulative probability and probability density functions versus applied K_J (generated using the Weibull stress versus applied load curves in Figure 24) are shown in Figures 25-26, respectively. Those probability curves indicate a predicted difference of 36 MPa$\sqrt{m}$ in median toughness between uniaxial (0:1) and biaxial (1:1) loading conditions for a shallow flaw located in fabrication weld material at -60°C.

The fracture toughness data obtained from this RPV shell cruciform test series were not sufficient to apply order statistics (see Eq. 8) for comparison with the predicted cumulative probability functions given in Figure 25. However, a new series of cruciform beam specimens, fabricated from another RPV shell, are scheduled to be tested jointly by the HSST Program and the European Commission Network for Evaluating Structural Components (NESC) in 2001 as a major element of the NESC-IV Project [26]. The NESC-IV Project should provide additional data needed for evaluating the Weibull cleavage fracture model when applied to shallow 3-dimensional flaws in RPV fabrication welds subjected to biaxial loading.

SUMMARY AND CONCLUSIONS

The HSST Program is engaged in development and experimental validation of cleavage fracture toughness models for shallow surface flaws located in RPV material and subjected to biaxial loading conditions. Objectives are being achieved through an integrated experimental and analytical approach. Material characterization testing and specialized toughness testing of larger cruciform beam specimen are part of the experimental program. *Local approach* methodology based on a three-parameter Weibull analytical model is used to correlate experimentally observed biaxial effects on fracture toughness. Preliminary conclusions derived from this study include the following:

- Results from uniaxial and biaxial tests performed on cruciform specimens from A533 B steels demonstrate that biaxial loading can have a pronounced effect on shallow-flaw fracture toughness in the lower-transition temperature region.

- The G-R-D calibration scheme was successfully applied in calibrations of three-parameter Weibull cleavage fracture toughness models for RPV steels.

- The Weibull model, with the hydrostatic stress criterion in place of the more commonly used maximum principal stress in the kernel of the Weibull stress integral definition, was shown to correlate experimentally observed biaxial effect in cruciform specimens in the lower-transition temperature region, thereby providing a scaling mechanism between uniaxial and biaxial loading states.

- Testing of 3-dimensional flaws in RPV fabrication weld material indicated that location of the cleavage initiation site(s) was dependent upon the biaxial loading ratio.

- Inspection of fracture surfaces from clad cruciform tests have produced experimental data that support the expected shift in location of cleavage initiation sites (due to a transition from uniaxial to biaxial loading) predicted by the Weibull stress density model. These experimental results highlight the potential utility of the Weibull stress density as a predictive tool for identifying locations along the 3-dimensional flaw perimeter with the highest probabilities of cleavage initiation for a given loading state.

- Cumulative probability functions predicted a difference of 36 MPa$\sqrt{m}$ in median toughness between uniaxial (0:1) and biaxial (1:1) loading conditions for a shallow flaw located in RPV fabrication weld material and tested at –60 °C. The current very limited data set (see Table 3) indicates a difference in median toughness of approximately 62 MPa$\sqrt{m}$; however, there are currently insufficient data available (2 uniaxial tests and 4 biaxial tests) to produce an experimentally-based estimate of mean or median shifts due to biaxiality with an acceptable level of statistical confidence.

The NESC-IV project should provide needed data for evaluating the Weibull cleavage fracture model when applied to shallow 3-dimensional flaws in RPV fabrication welds subjected to biaxial loading.

References

[1] Theiss, T. J. and Shum, D. K. M., "Experimental and Analytical Investigation of the Shallow-Flaw Effect in Reactor Pressure Vessels," USNRC Report NUREG/CR-5886 (ORNL/TM-12115), Oak Ridge National Laboratory, Oak Ridge, Tennessee/USA, July 1992.

[2] Theiss, T. J., Bass, B. R., Bryson, Jr., J. W., McAfee, W. J., Nanstad, R. K., Pennell, W. E., and Rao, M. C., "Initial Results of the Influence of Biaxial Loading on Fracture Toughness," USNRC Report NUREG/CR-6036 (ORNL/TM-12349), Oak Ridge National Laboratory, Oak Ridge, Tennessee/USA, June 1993.

[3] McAfee, W. J., Bass, B. R., and Bryson, Jr., J. W., "Development of a Methodology for the Assessment of Shallow-Flaw Fracture in Nuclear Reactor Pressure Vessels," *ASME Pressure Vessel and Piping Conference*, Orlando, Florida/USA, July 27-31, 1997, PVP-Vol. 346, pp. 85-94.

[4] Pennell, W. E., Bass, B. R., Bryson, Jr., J. W. , Dickson, T. L., and Merkle, J. G., "Preliminary Assessment of the Effects of Biaxial Loading on Reactor Pressure Vessel Structural-Integrity-Assessment Technology," *Proceedings of 4th ASME/JSME International Conference in Nuclear Engineering*, New Orleans, Louisiana/USA, March 10-14, 1996.

[5] McAfee, W. J., Bass, B. R., Bryson, Jr., J. W., and Pennell, W. E., "Biaxial Loading Effects on Fracture Toughness of Reactor Pressure Vessel Steel," USNRC Report NUREG/CR-6273 (ORNL/TM-12866), Oak Ridge National Laboratory, Oak Ridge, Tennessee/USA, March 1995.

[6] Bass, B. R., Bryson, Jr., J. W. , Theiss, T. J., and Rao, M. C., "Biaxial Loading and Shallow-Flaw Effects on Crack-Tip Constraint and Fracture Toughness," USNRC Report NUREG/CR-6132 (ORNL/TM-12498), Oak Ridge National Laboratory, Oak Ridge, Tennessee/USA, January 1994.

[7] Bass, B. R., McAfee, W. J., Bryson, Jr., J. W., and Pennell, W. E. "Determination of Cladding Effects on Shallow-Flaw Fracture Toughness of Reactor Pressure Vessel Steel under Prototypic Biaxial Loading," *5th International Conference on Nuclear Engineering*, Nice, France, May 26-30, 1997.

[8] Bass, B. R., McAfee, W. J., Williams, P. T., and Pennell, W. E., "Evaluation of Constraint Methodologies Applied to a Shallow-Flaw Cruciform Bend Specimen tested under Biaxial Loading Conditions," *Fatigue, Fracture, and High Temperature Design Methods in Pressure Vessels and Piping, ASME/JSME Joint Pressure Vessels and Piping Conference*, San Diego, California/USA, July 26-30, 1998, PVP-Vol. 365, pp. 11-25.

[9] Bass, B. R., McAfee, W. J., Williams, P. T., and Pennell, W. E., "Fracture Assessment of Shallow-Flaw Cruciform Beams tested under Uniaxial and Biaxial Loading Conditions," *Nuclear Engineering and Design*, Vol. 188, No. 3, 1999, pp. 259-288.

[10] ASTM E 1921-97, Test Method for the Determination of Reference Temperature, T_o, for Ferritic Steels in the Transition Region, American Society for Testing and Materials, West Conshohocken, PA, 1998.

[11] Garwood, S. J., "The Significance of Biaxial Loading on the Fracture Performance of a Pressure Vessel Steel," *Pressure Vessel Integrity, ASME Pressure Vessels and Piping Conference,* PVP-Vol. 213/MPC-Vol. 32, 1991, pp. 113-123.

[12] Bass, B. R., et al., "Research Results Supporting Enhanced Fracture Analysis Methods for Nuclear Reactor Pressure Vessels," USNRC Report NUREG/CR-6657 (ORNL/TM-1999/270), Oak Ridge National Laboratory, Oak Ridge, Tennessee/USA (in publication).

[13] *ABAQUS Theory Manual, Version 5.7*, Hibbit, Karlson and Sorensen, Inc., Providence, RI, 1997.

[14] Ruggieri, C, and Dodds, R.H., "Numerical Computation of Probabilistic Fracture Parameters Using WSTRESS," *Engng Computat*, Vol. 15, 1998, pp. 49-73.

[15] Freudenthal, A. M., "Statistical Approach to Brittle Fracture," *Fracture: An Advanced Treatise, Vol. 2, Mathematical Fundamentals*, ed. H. Liebowitz, Academic Press, New York, 1968, pp. 591-619.

[16] Dortmans, L., Thiemeier, T., Brückner-Foit, A., and Smart, J., "WELFEP: A Round Robin for Weakest-Link Finite Element Postprocessors," *Journal of the European Ceramic Society*, 0955-2219/93/S6.00, Elsevier Science Publishers Ltd, England, 1993.

[17] Hellen, T. K. and Blackburn, W. S., "The Calculation of Stress Intensity Factors for Combined Tension and Shear Loading," *International Journal of Fracture*, Vol. 11, 1975, pp. 605-617.

[18] Lamon, J. and Evans A. G., "Statistical Analysis of Bending Strengths for Brittle Solids: A Multiaxial Fracture Problem," *Journal of the American Ceramic Society,* Vol. 66, 1983, pp. 177-182.

[19] Williams, P.T., Bass, B.R., and McAfee, W.J., "Application of the Weibull Methodology to a Shallow-Flaw Cruciform Bend Specimen Tested under Biaxial Loading Conditions," *Fatigue and Fracture Mechanics*, STP 1389, American Society of Testing and Materials, West Conshohocken, PA, 2000.

[20] Gao, X., Ruggieri, C. and Dodds, R. "Calibration of Weibull Stress Models Using Fracture Toughness Data," *Int. J. Frac.* **92**, (1998) 175-200.

[21] Gao, X. and Dodds, Jr., R.H., "A Weibull Stress Model to Predict Cleavage Fracture in Plates Containing Surface Cracks," *Fatigue & Fracture of Engineering Materials and Structures* **22**, (1999) 481-493.

[22] Larsson, S. G. and Carlson, A. J., "Influence of Non-Singular Stress Terms and Specimen Geometry on Small Scale Yielding of Crack-Tips in Elastic-Plastic Materials," *Journal of the Mechanics and Physics of Solids*, Vol. 21, 1973, pp. 447-473.

[23] Rice, J. R., "Limitations to the Small Scale Yielding Approximation for Crack-Tip Plasticity," *Journal of the Mechanics and Physics of Solids,* Vol. 22, 1974, pp. 17-26.

[24] Merkle, J. G., Wallin, K., and McCabe, D. E., 1998, Technical Basis for an ASTM Standard on Determining the Reference Temperature, T_0, for Ferritic Steels in the Transition Range, USNRC Report NUREG/CR-5504 (ORNL/TM-13631), Oak Ridge National Laboratory, Oak Ridge, TN.

[25] Gao, X., Dodds, Jr., R. H., Tregoning, R. L., Joyce, J. A., and Link, R. E., 1999, "A Weibull Stress Model to Predict Cleavage Fracture in Plates Containing Surface Cracks," Fatigue and Fracture of Engineering Materials and Structures, **22**, pp. 481-493.

[26] Bass, B. R., Williams, P. T., and Pugh, C. E., *NESC IV Project: Biaxial Fracture Toughness Testing and Analysis of Shallow Flaws in RPV Materials*, Proposed Work Program, NESC DOC MAN(00)08, October 2000.

Table 1. Deep-Flaw SE(B) Data for Longitudinal Weld

Specimen ID	Test Temperature (°C)	*a/W*	Failure Load (kN)	K_J (MPa-√m)
SBD1	-62.2	0.5	65.8	161.1
SBD2	-62.2	0.5	35.4	71.5
SBD3	-62.2	0.5	42.2	85.9
SBD4	-62.2	0.5	48.9	103.5
SBD5	-62.2	0.5	42.5	92.5
SBD6	-62.2	0.5	52.9	178.8
SBD7	-62.2	0.5	56.6	121.3
SBD8	-62.2	0.5	56.7	131.8

Table 2. Shallow-Flaw SE(B) Data for Longitudinal Weld

Specimen ID	Test Temperature (°C)	*a/W*	Failure Load (kN)	K_J (MPa-√m)
SBS1	-62.2	0.2	149.3	169.2
SBS2	-62.2	0.2	152.4	175.4
SBS3	-62.2	0.2	155.5	192.2
SBS4	-62.2	0.2	149.5	188.6
SBS5	-62.2	0.2	151.4	220.9
SBS6	-62.2	0.2	139.6	155.6
SBS7	-62.2	0.2	96.6	83.4
SBS8	-62.2	0.2	138.1	148.5

Table 3. Estimated Toughness Values for Clad Cruciform Beams Fabricated from Longitudinal Weld Material

Specimen ID[1]	Biaxial Ratio	Temperature (°C)	T-RT_{NDT}[2] (°C)	T-T_0[3] (°C)	Longitudinal Failure Moment (kN-m)	Fracture Toughness (MPa-√m)
CBL11-3	(0:1)	-56.5	3.4	11.1	139.6	162.4
CBL11-2	(0:1)	-63.5	-3.5	4.2	133.4	149.5
CBL11-1	(1:1)	-62.5	-2.6	5.1	122.1	110.9
CBC22	(1:1)	-42.7	-2.7	0.7	133.7	133.4[4]
CBL17	(1:1)	-63.9	-3.9	3.8	96.1	82.1[4]
CBL25	(1:1)	-65.4	-5.8	1.9	113.2	105.4[4]
CBL15	(1:1)	-63.2	-3.2	4.5	85.4	72.1[4]

[1] CBL = Clad Beam Longitudinal Weld
CBC = Clad Beam Circumferential Weld
[2] Longitudinal Weld: RT_{NDT} = -60°C
Circumferential Weld RT_{NDT} = -40°C
[3] Longitudinal Weld T_0 = -67.7°C
Circumferential Weld T_0 = -43.4°C assuming initiation site near surface
[4] Estimated based on assumed initiation site location

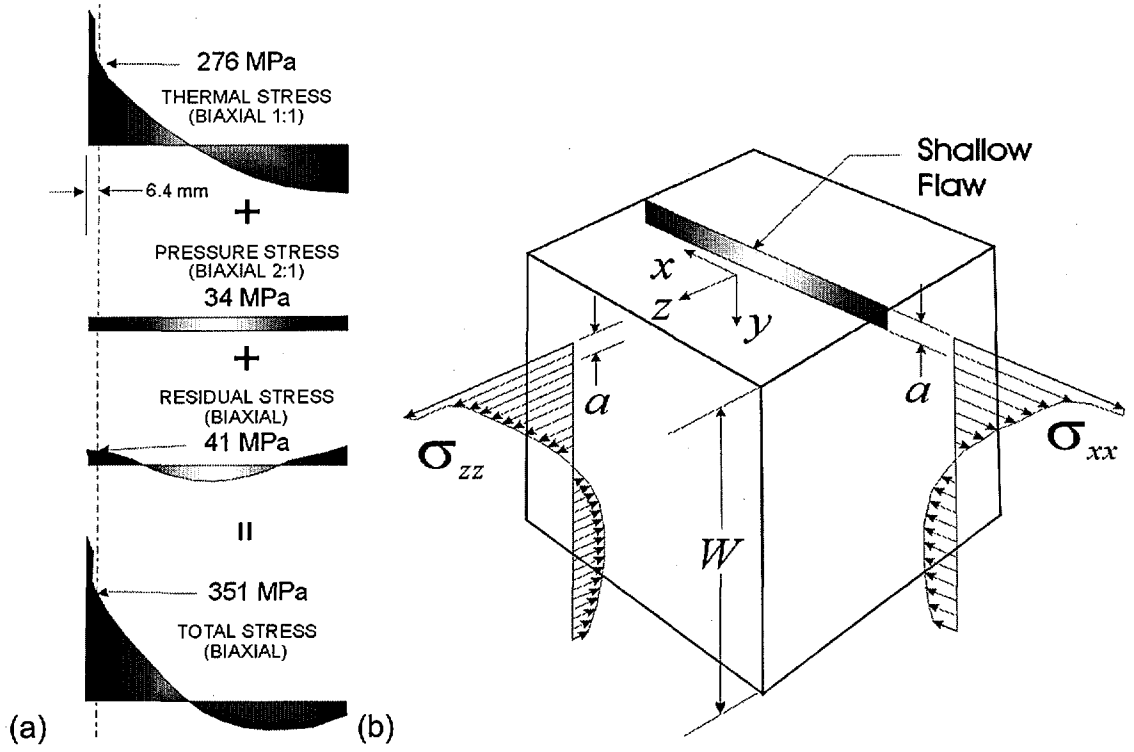

Figure 1. Pressurized thermal shock loading produces a nonlinear biaxial stress state in a pressure vessel wall: (a) contributions of thermal, pressure, and residual stresses and (b) total complex state of stress applied to a shallow surface flaw.

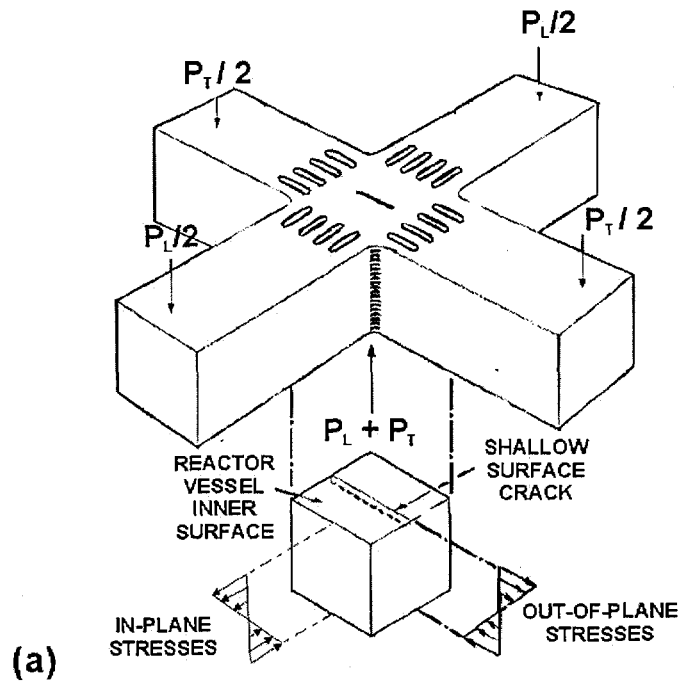

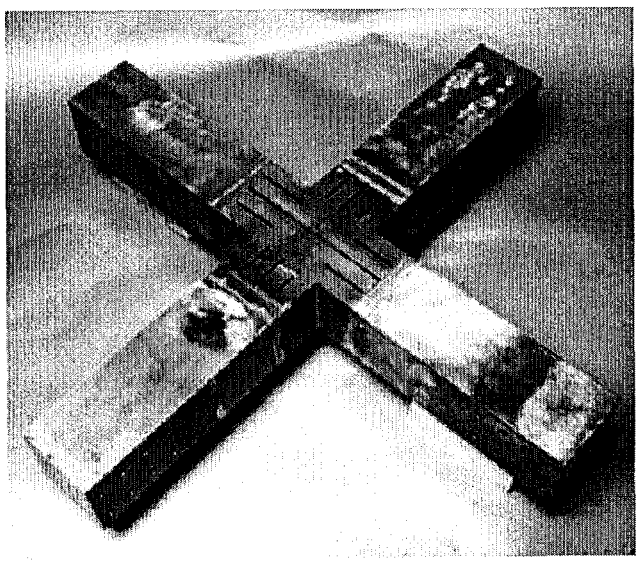

Figure 2. Shallow-flaw cruciform bend specimen developed in the HSST Program: (a) conceptual features of test specimen subjected to biaxial loading; (b) cruciform specimen fabricated from heat-treated HSST Plate 14 material.

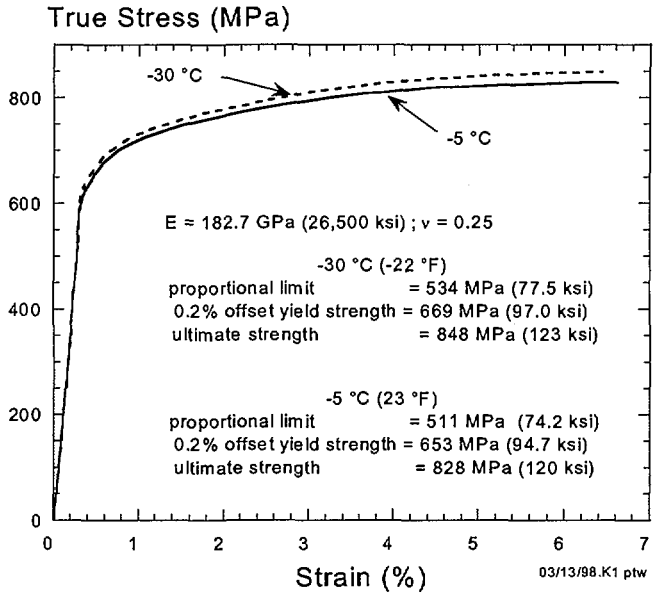

Figure 3. Stress-strain behavior for HSST Plate 14 RPV steel.

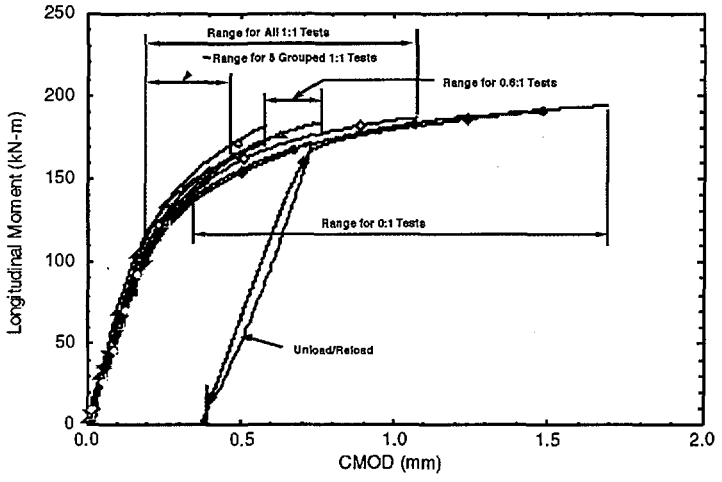

Figure 4. Comparison of CMOD responses for HSST Plate 14 cruciform specimens at a nominal test temperature of -5 °C (23 °F) for biaxial load ratios of (0:1), (0.6:1), and (1:1).

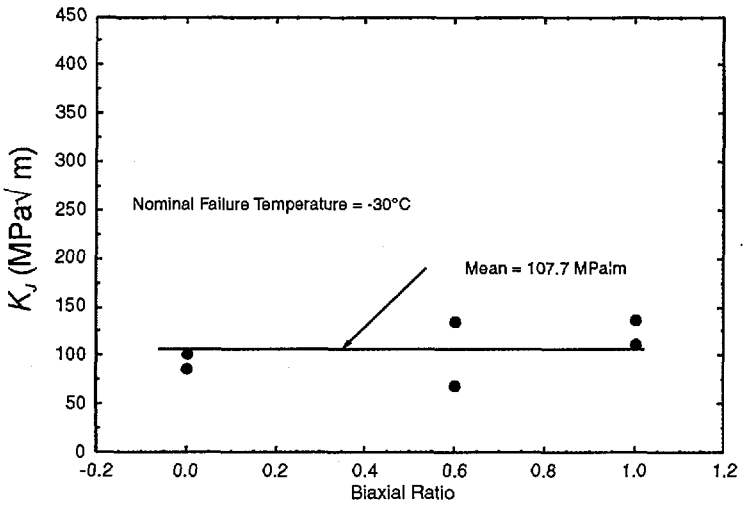

Figure 5. Fracture toughness data determined for heat-treated HSST Plate 14 tested at -30° C indicating no effect of biaxial load ratio on fracture toughness at the lower-shelf temperature.

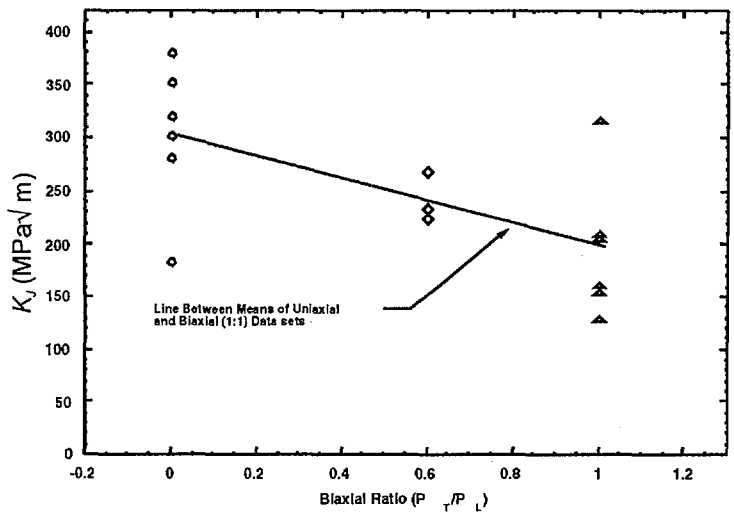

Figure 6. The effect of biaxial load ratio on fracture toughness determined for heat-treated HSST Plate 14 tested at -5 °C.

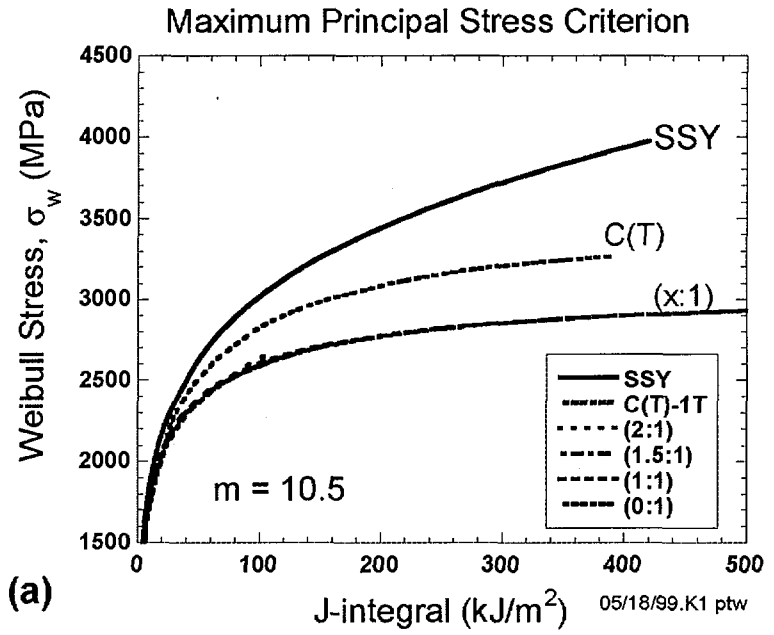

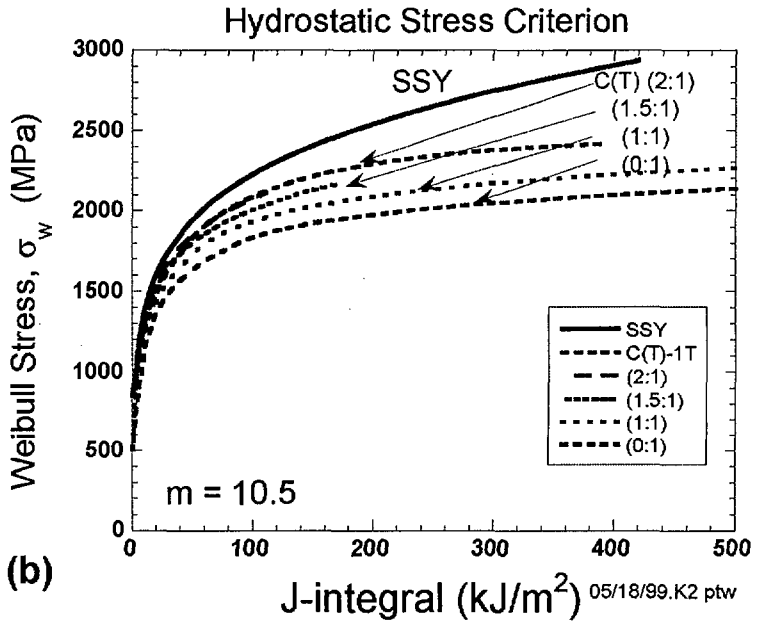

Figure 7. Sensitivity of Weibull stress to variations in constraint levels for (a) maximum principal stress criterion and (b) hydrostatic stress criterion at *m* = 10.5 for HSST Plate 14 cruciform bend specimen (straight flaw).

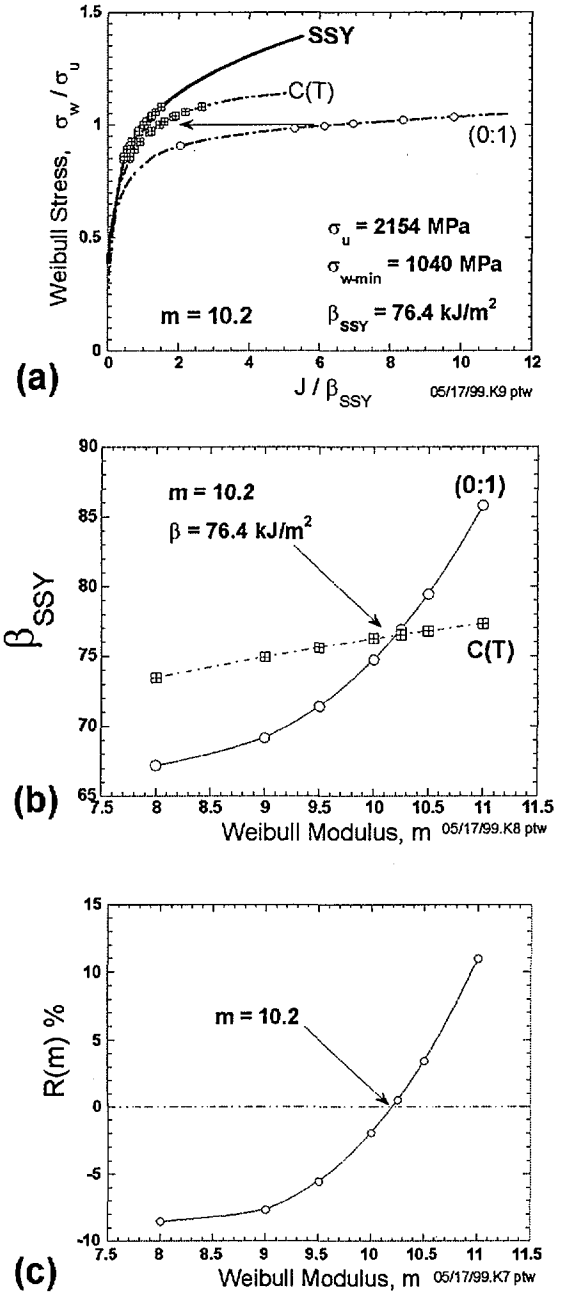

Figure 8. Calibration results using (high-constraint) C(T) and (low-constraint) uniaxial (0:1) cruciform toughness data: (a) constraint correction to SSY, (b) β_{SSY} versus *m*, and (c) error function *R(m)* versus *m*.

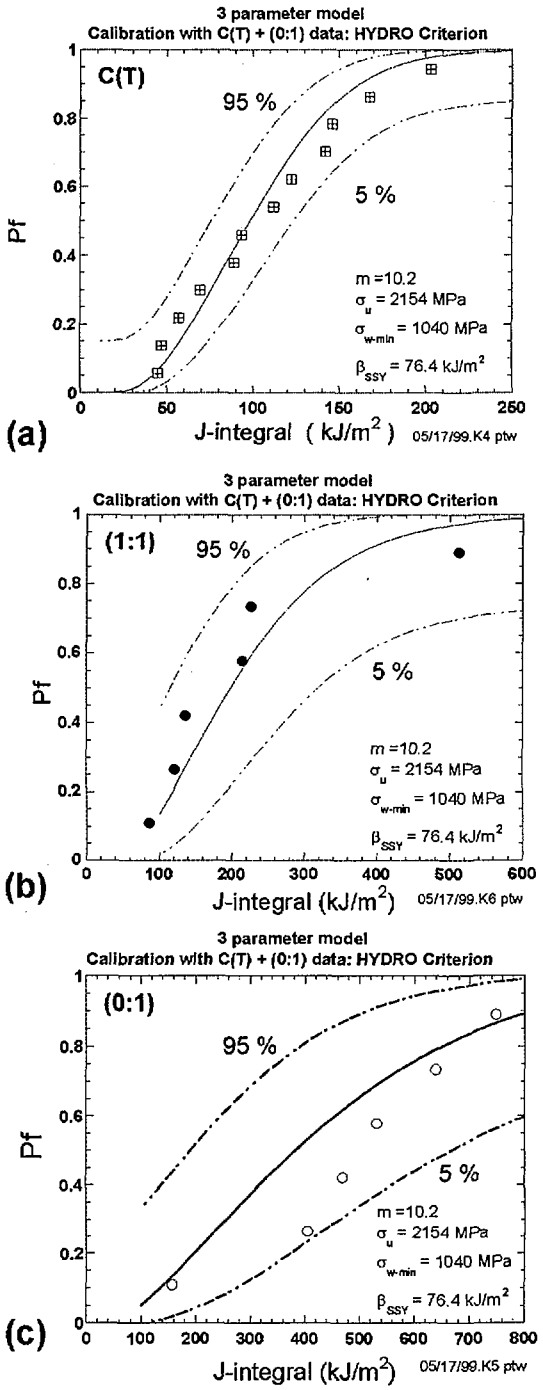

Figure 9. Failure probabilities resulting from calibration using hydrostatic-stress criterion with (high-constraint) C(T) and (low-constraint) uniaxial (0:1) cruciform toughness data, three-parameter Weibull model: m = 10.2, σ_u = 2154, and $\sigma_{w\text{-}min}$ = 1040 MPa: (a) C(T) correlation, (b) equibiaxial (1:1) correlation, and (c) uniaxial (0:1) correlation.

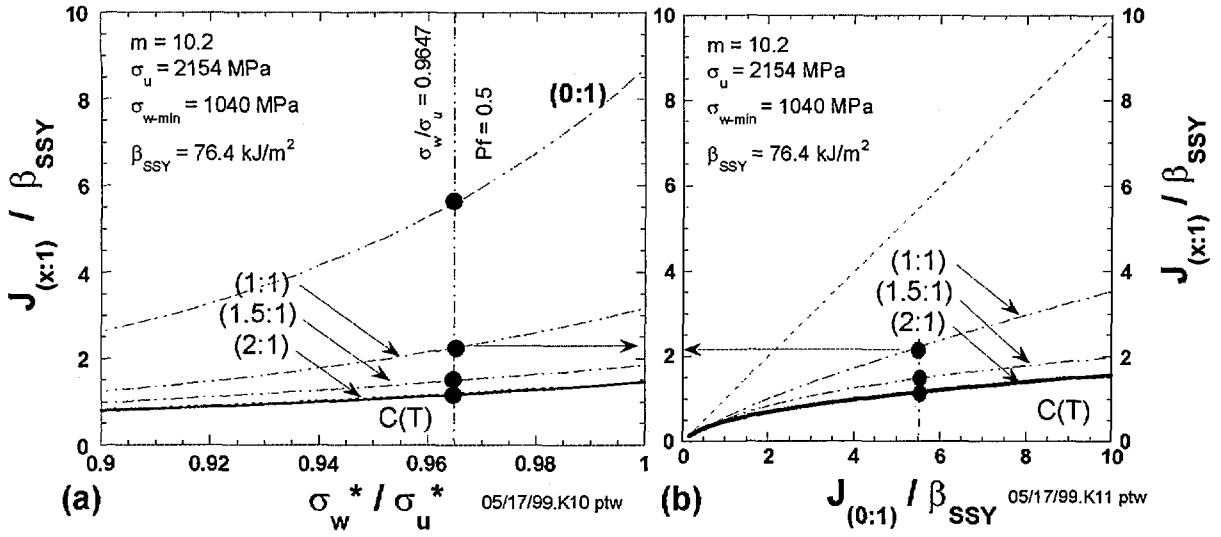

Figure 10. Biaxial scaling model for variations in biaxiality in terms of *J*-integral.

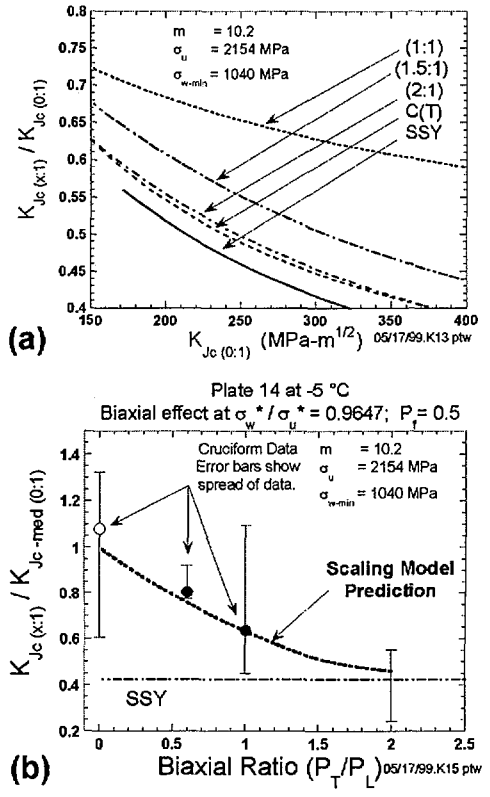

Figure 11. Biaxial scaling model for variations in biaxiality in terms of toughness ratios: (a) variation with uniaxial (0:1) toughness and (b) variation with biaxiality ratio for P_f = 0.5. Experimental points are the medians of the test data normalized by the predicted median of the uniaxial (0:1) cruciform.

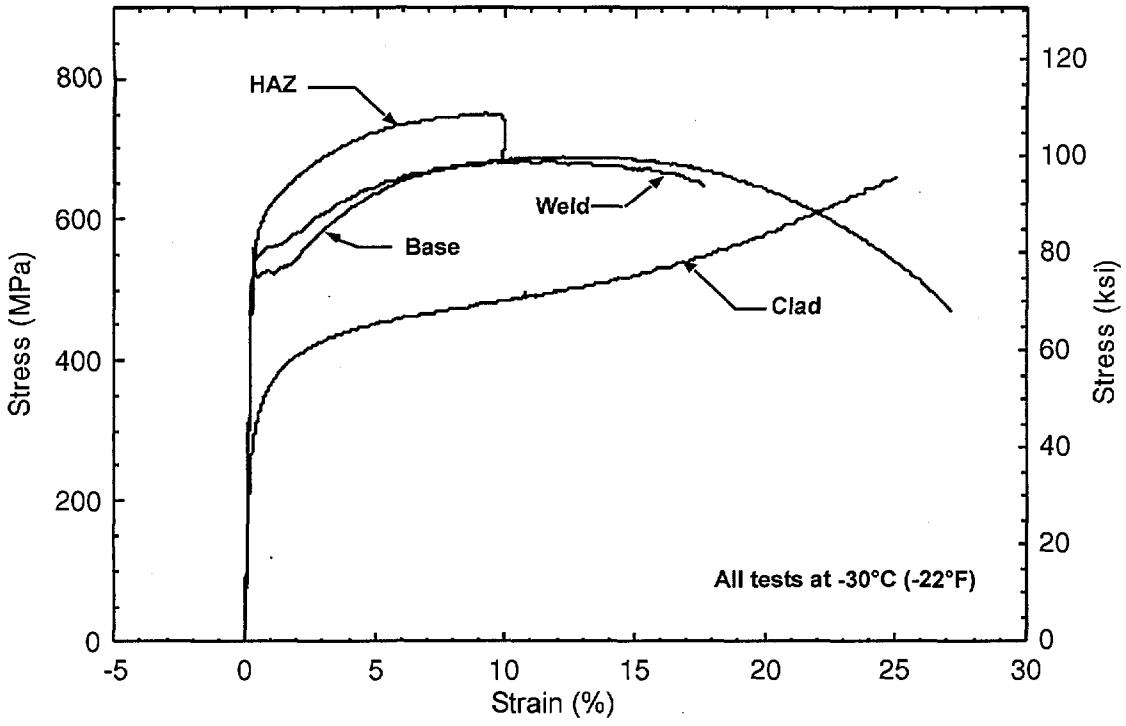

Figure 12. Comparison of the stress-strain characteristics of the component materials in the clad-cruciform beam specimens.

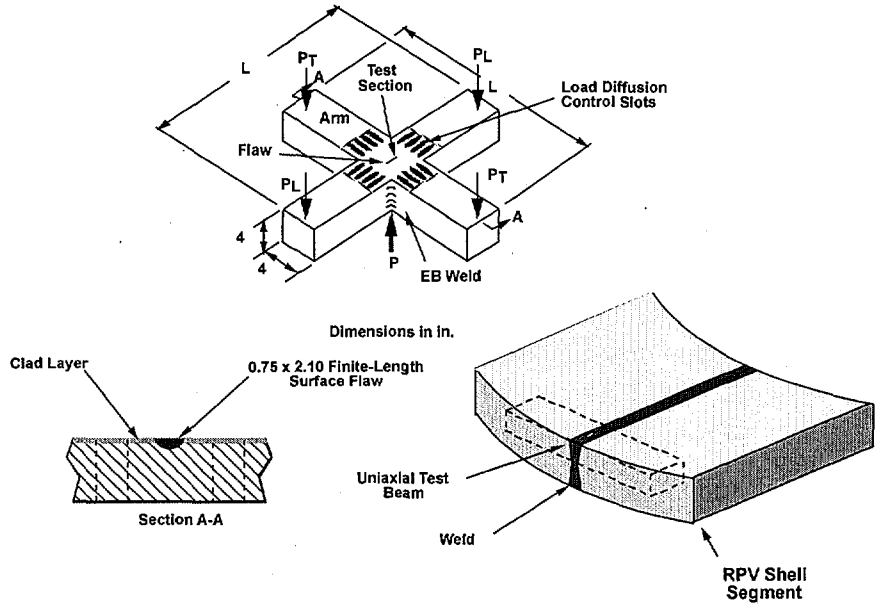

Figure 13. Finite-length flaw specimens cut from an RPV shell segment are used to investigate the effect of the clad layer and specimen size on initiation behavior of prototypic RPV welds.

ORNL Photo 323603

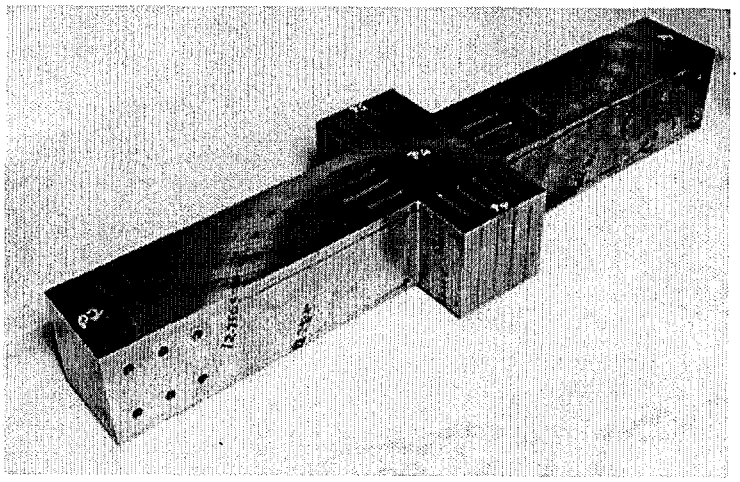

(a)

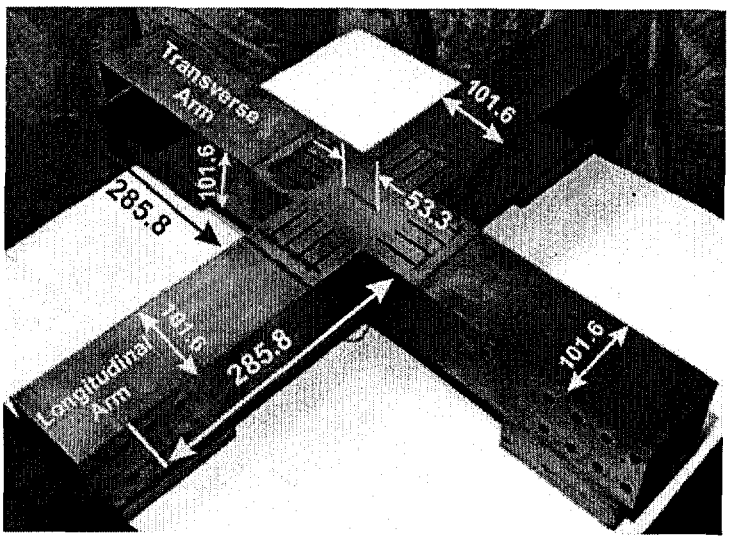

(b)

Figure 14. RPV clad-cruciform specimens are fabricated from either a machined test section or a uniaxial beam. After fatigue pre-cracking, transverse beam arms are electron beam (EB) -welded to form a cruciform specimen. Relevant dimensions of the cruciform specimen are given in mm.

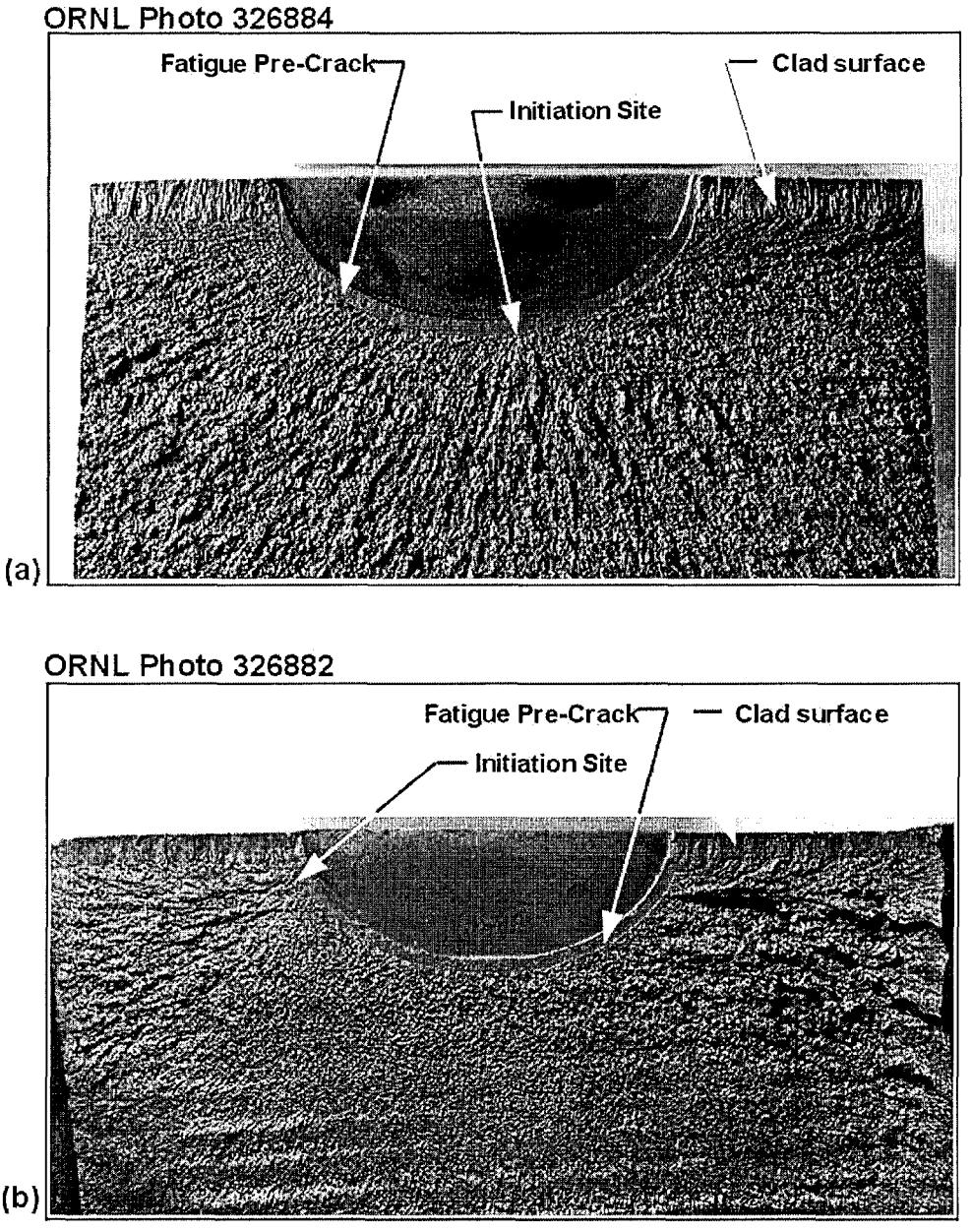

Figure 15. Fracture surface for (a) specimen CBL 11-3 showing initiation site location; test performed at –56.6°C under uniaxial (0:1) loading; (b) specimen CBL 11-1 showing initiation site location; test performed at –62.6°C under biaxial (1:1) loading.

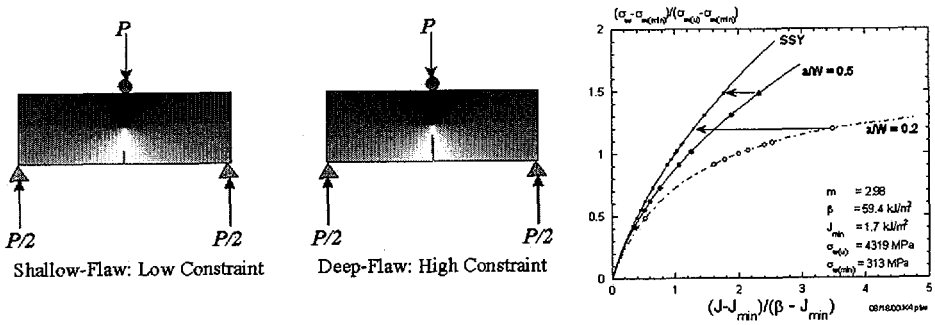

$$P_f = 1 - \exp\left[-\left(\frac{J_{SSY} - J_{SSY(\min)}}{\beta - J_{SSY(\min)}}\right)^2\right] = 1 - \exp\left[-\left(\frac{\sigma_w - \sigma_{w(\min)}}{\sigma_u - \sigma_{w(\min)}}\right)^m\right]$$

Figure 16. Calibration with low- and high-constraint SE(B) specimens under uniaxial loading (3-point bending) establishes the Weibull model parameters m, σ_u, $\sigma_{w(\min)}$, β, and $J_{SSY(\min)}$ for a given material (RPV longitudinal weld).

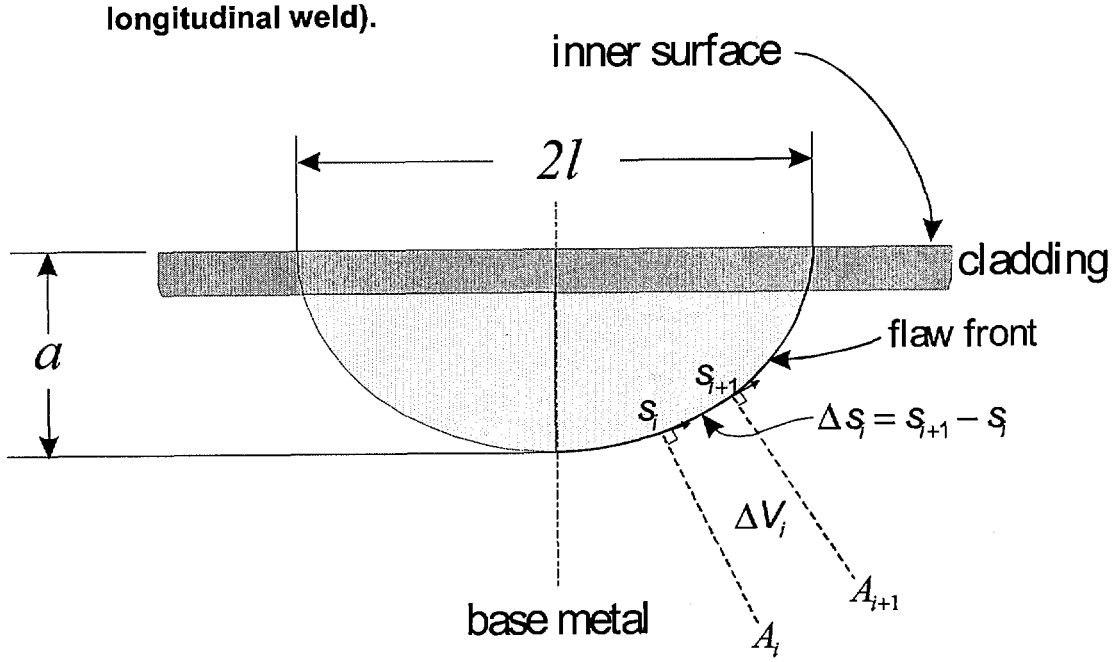

Figure 17. Model for semi-elliptical surface flaw to calculate Weibull stress density.

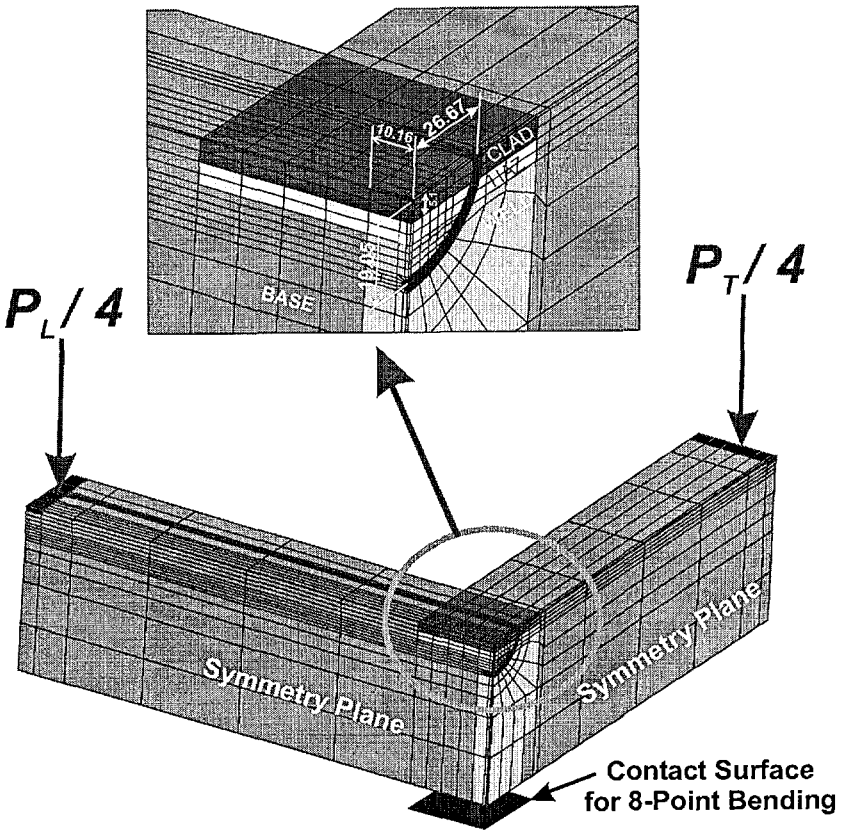

Figure 18. Finite-element 1/4 model with bending loads applied as uniform surface pressures at ends of longitudinal and transverse beam arms. Rigid contact surface under test section completes statically-determinate boundary conditions that simulate 8-point bending.

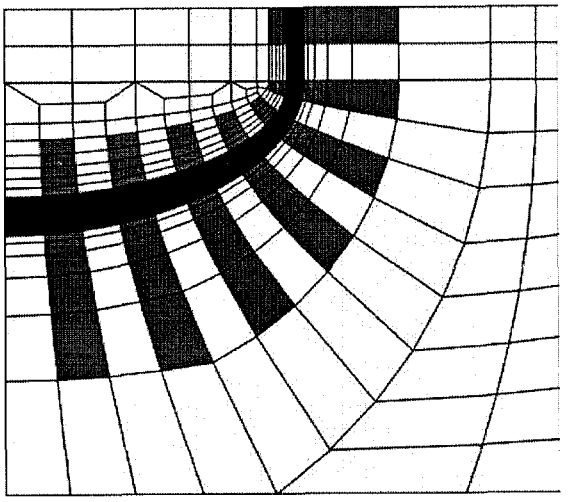

Figure 19. Layout of element partitions for the calculation of a generalized Weibull density function as a function of position along the flaw-front of an RPV clad cruciform specimen.

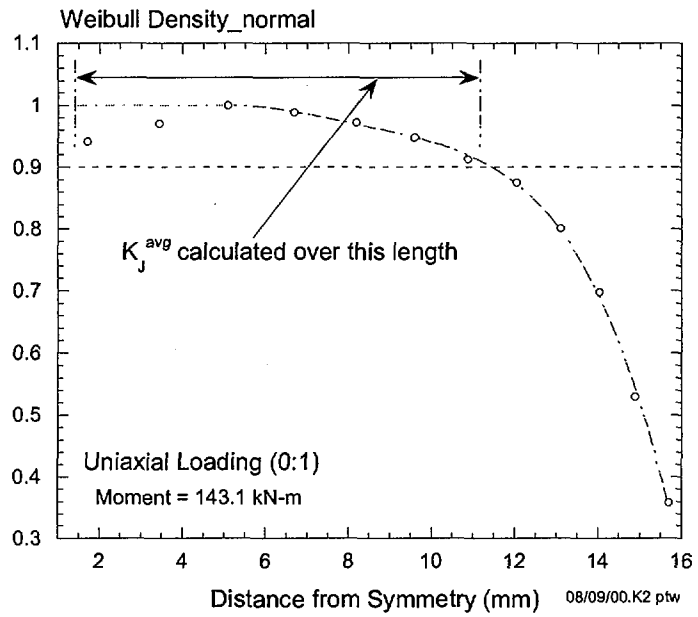

Figure 20. Normalized Weibull stress density versus distance from symmetry plane for an RPV clad cruciform beam subjected to a uniaxial moment loading of 143.1 kN-m.

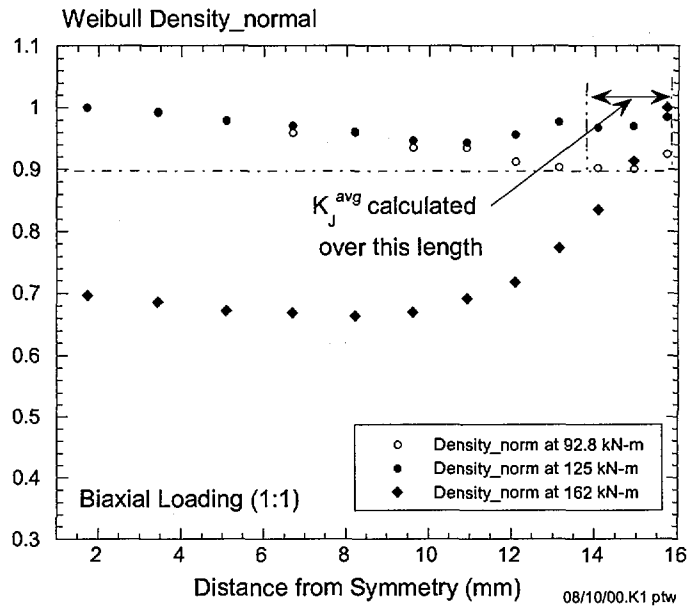

Figure 21. Normalized Weibull stress density versus distance from symmetry plane for an RPV clad cruciform beam subjected to biaxial moment loading.

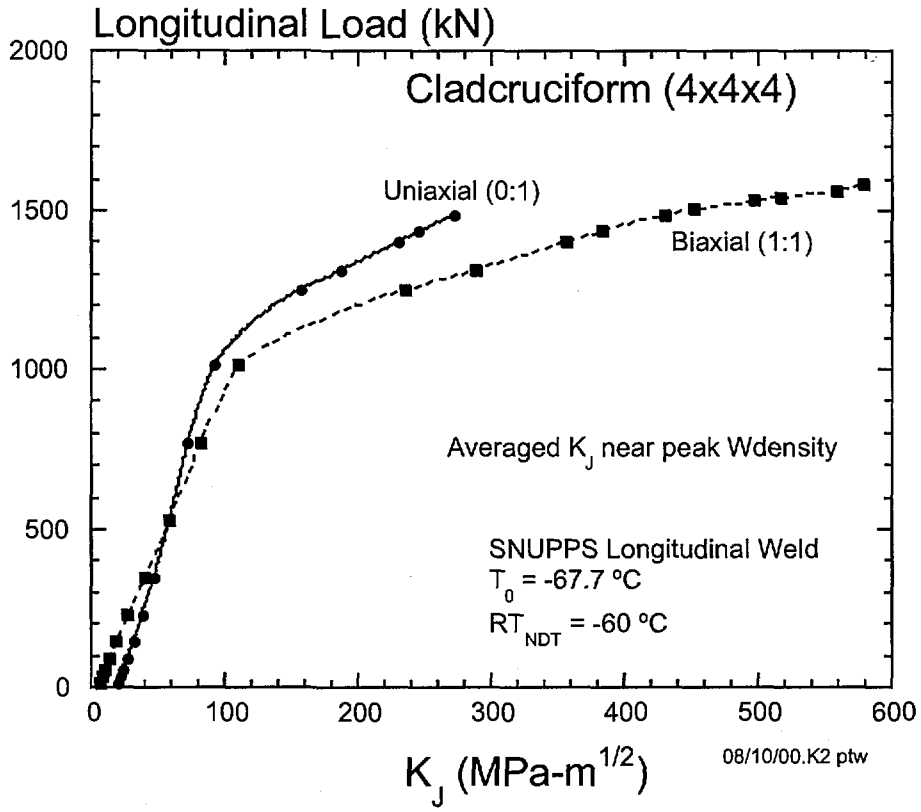

Figure 22. Applied longitudinal load versus applied K_J for an RPV clad cruciform specimen subjected to uniaxial (0:1) and biaxial (1:1) loading at - 60°C.

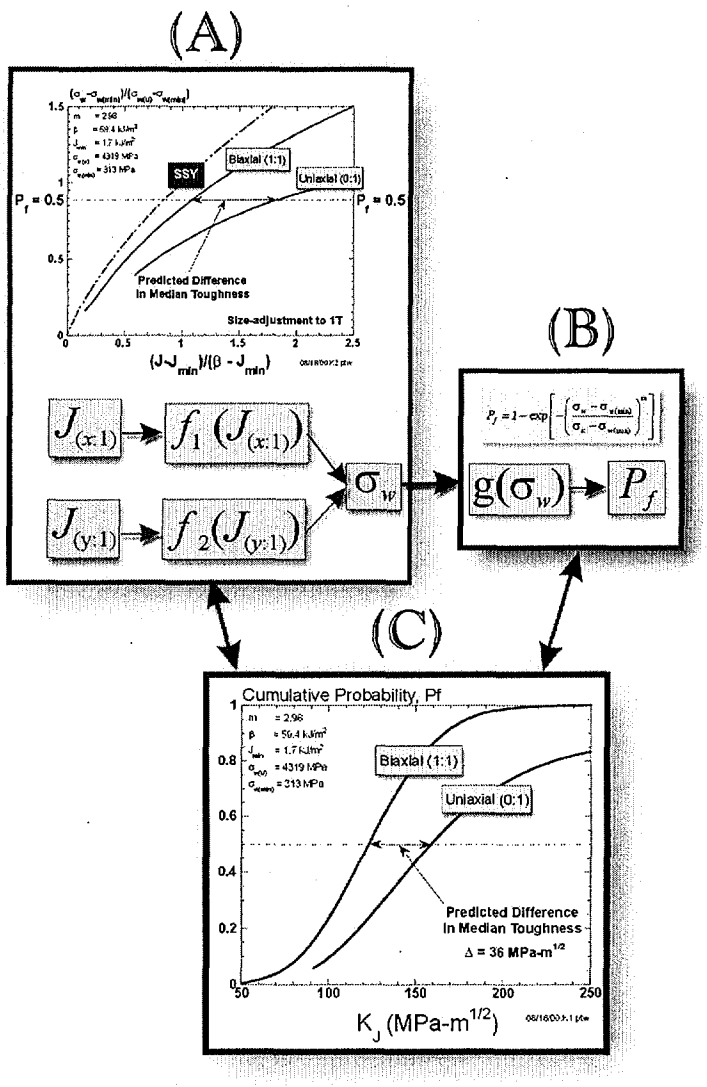

Figure 23. Schematic diagram depicting the linkage between essential elements of the analysis process: (a) the unique functional relationship between the applied load (in terms of J or K_J) and the Weibull stress, σ_w, for a given constraint condition (b) the Weibull stress and the cumulative probability of initiation, P_f, defined by the Weibull model parameters. and (c) the resulting toughness scaling curves for varying levels of constraint.

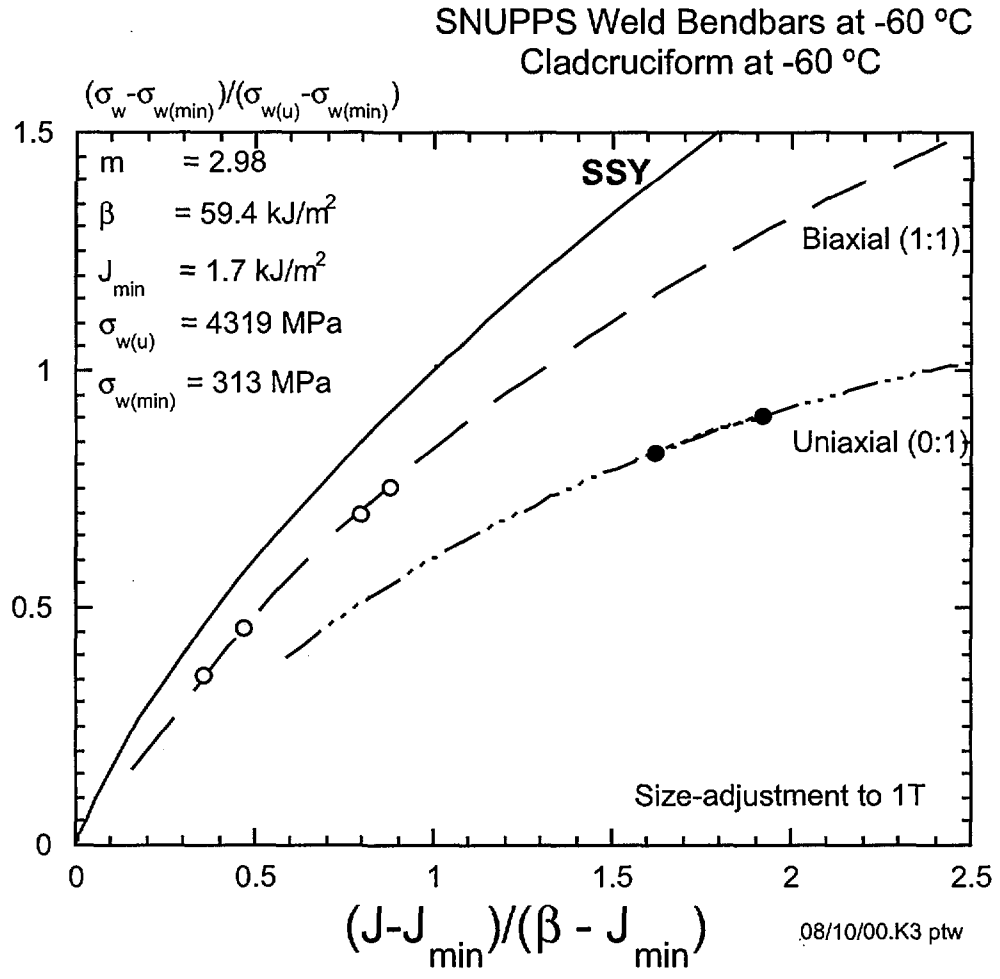

Figure 24. Normalized Weibull stress versus normalized applied *J* for RPV clad cruciform specimen subjected to uniaxial (0:1) and biaxial (1:1) loading at - 60°C.

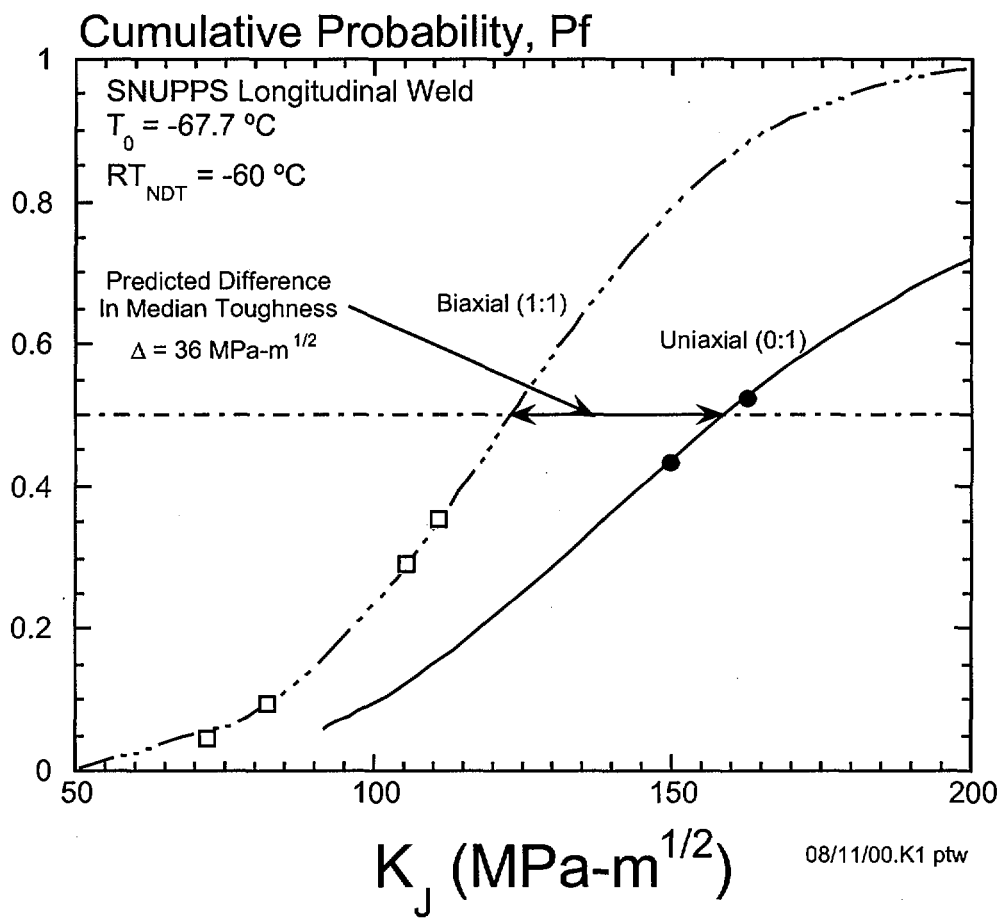

Figure 25. Cumulative probability versus applied K_J for RPV clad cruciform specimen subjected to uniaxial (0:1) and biaxial (1:1) loading at - 60°C.

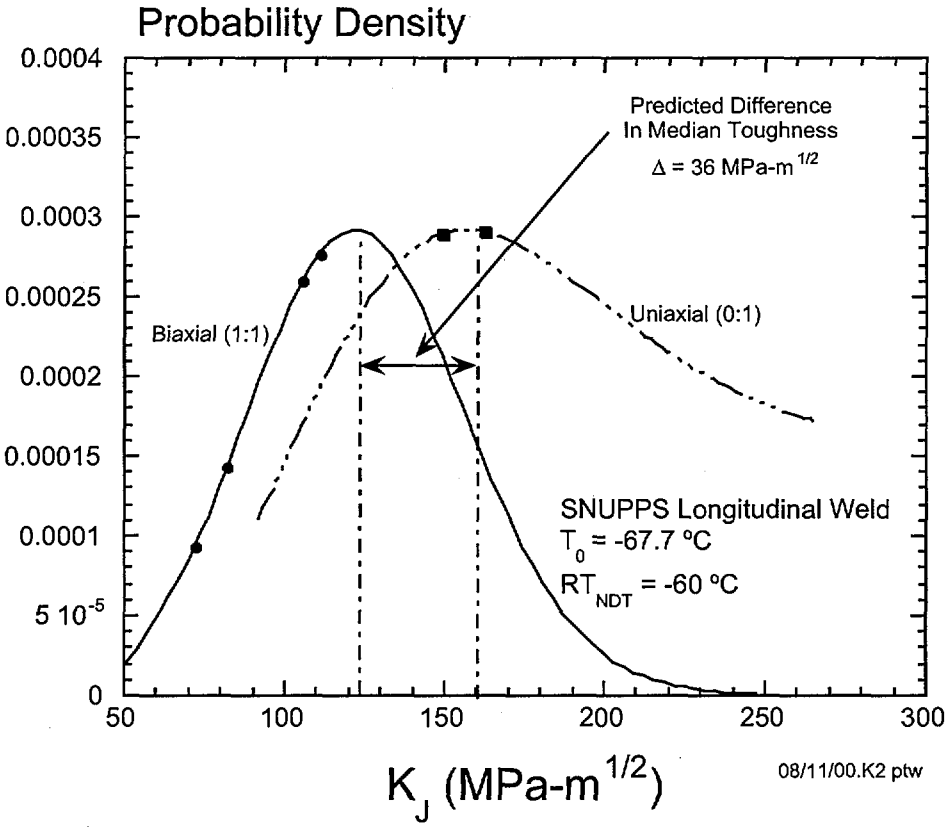

Figure 26. Probability density versus applied K_J for RPV clad cruciform specimen subjected to uniaxial (0:1) and biaxial (1:1) loading at - 60°C.